Journal of Hazardous Materials 461 (2024) 132733

Contents lists available at ScienceDirect

Journal of Hazardous Materials

journal homepage: www.elsevier.com/locate/jhazmat

Macrophage-derived MMP12 promotes fibrosis through sustained damage to endothelial cells

Xinbei Zhou [a,b,1], Cong Zhang [a,b,1], Shaoqi Yang [a,b,1], Liliang Yang [a], Wei Luo [a,c], Wei Zhang [a], Xinxin Zhang [a], Jie Chao [a,b,c,d,*]

[a] Jiangsu Provincial Key Laboratory of Critical Care Medicine, Zhongda Hospital, Department of Physiology, School of Medicine, Southeast University, Nanjing, Jiangsu, 210009, China
[b] Key Laboratory of Environmental Medicine Engineering, Ministry of Education, School of Public Health, Southeast University, Nanjing, Jiangsu, 210009, China
[c] Jiangsu Key Laboratory of Molecular and Functional Imaging, Department of Radiology, Zhongda Hospital, Medical School of Southeast University, Nanjing 210009, China
[d] School of Medicine, Xizang Minzu University, Xianyang, Shanxi, 712082, China

HIGHLIGHTS

- This study investigated the role of new member of matrix metalloproteinases in the development of silicosis.
- The interactions between extracellular matrix and cells in a silicosis model was investigated.
- Multi-omics sequencing were combined to investigate the potential mechanisms of silicosis.

GRAPHICAL ABSTRACT

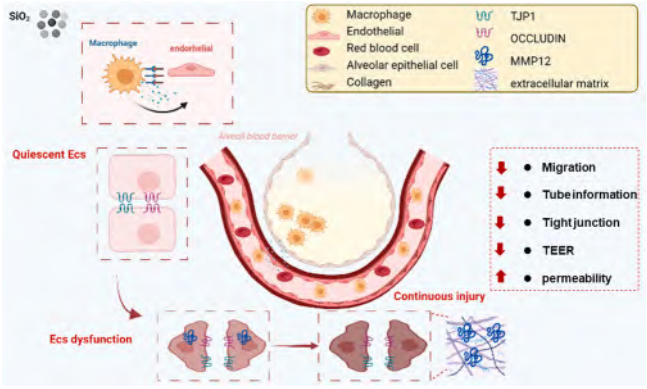

ARTICLE INFO

Editor: Dr. S.Y Chen

Keywords:
Silicosis
Pulmonary fibrosis

ABSTRACT

Macrophages are essential for the maintenance of endothelial cell function. However, the potential impact and mechanisms of crosstalk between macrophages and endothelial cells during silicosis progression remain unexplored. To fill this knowledge gap, a mouse model of silicosis was established. Single cell sequencing, spatial transcriptome sequencing, western blotting, immunofluorescence staining, tube-forming and wound healing assays were used to explore the effects of silicon dioxide on macrophage-endothelial interactions. To investigate

Abbreviations: ARRIVE, animal research in vivo experimental report; ATCC, American Type Culture Collection; BCA, bicinchoninic acid; CM, conditioned medium; Ct, cycle threshold; ECM, extracellular matrix; HUVEC, Human Umbilical Vein Endothelial Cell; IPF, idiopathic pulmonary fibrosis; MMP, matrix metalloproteinase; PBS, phosphate-buffered saline; PCA, principal component analysis; PE150, 150-bp paired end; PMA, phorbol acetate; qRT-PCR, real-time quantitative RT-PCR; TEER, transendothelial electrical resistance; t-SNE, t-distributed stochastic neighbor embedding; UMI, Unique Molecular Identifier.

* Correspondence to: Department of Physiology, School of Medicine, Southeast University, 87 Dingjiaqiao Rd, Nanjing, Jiangsu, 210009, China.
E-mail address: chaojie@seu.edu.cn (J. Chao).

[1] These authors contribute equally to this work.

https://doi.org/10.1016/j.jhazmat.2023.132733
Received 27 April 2023; Received in revised form 16 September 2023; Accepted 4 October 2023
Available online 6 October 2023

Macrophage-endothelial interactions
Extracellular matrix (ECM)

the mechanism of macrophage-mediated fibrosis, MMP12 was specifically inactivated using siRNA and pharmacological approaches, and macrophages were depleted using disodium chlorophosphite liposomes. Compared to the normal saline group, the silica dust group showed altered macrophage-endothelial interactions. Matrix metalloproteinase family member MMP12 was identified as a key mediator of the altered function of macrophage-endothelial interactions after silica exposure, which was accompanied by pro-inflammatory macrophage activation and fibrotic progression. By using ablation strategies, macrophage-derived MMP12 was shown to mediate endothelial cell dysfunction by accumulating on the extracellular matrix. During the inflammatory phase of silicosis, MMP12 secreted by pro-inflammatory macrophages caused decreased endothelial cell viability, reduced migration, decreased trans-endothelial resistance and increased permeability; while during the fibrotic phase, macrophage-derived MMP12 sustained endothelial cell injury through accumulation on the extracellular matrix.

1. Introduction

Silicosis is characterized by diffuse fibrosis of lung tissues with systemic inflammation caused by long-term inhalation of free silica dust [1]. The specific mechanisms underlying the development of silicosis have not been elucidated; generally, fibroblasts are considered to be central players in pulmonary fibrosis, but it has also been recognized that the absence of endothelial cells and uncontrolled angiogenesis are key biological processes underlying pulmonary fibrosis [2-4]. Under physiological conditions, vascular endothelial cells support fibroblast development and regeneration, whereas in response to exogenous stimuli, endothelial cells are activated and vascular integrity is disrupted, directly initiating an inflammatory response or promoting an already existing inflammatory response. Endothelial cells can also mediate vasorelaxation and reduction of angiogenesis by increasing myofibroblasts and promoting the recruitment of immune cells; or can contribute to the development and progression of fibrosis by secreting pro-fibrotic mediators [5]. Moreover, in idiopathic fibrotic lungs, endothelial cells and macrophages have been shown to have tight spatial connections and multi-directional intercellular communication [6,7]. Thus, accumulating evidence supports a key underlying role for macrophage-endothelial interactions in the development of silica-associated fibrosis.

Macrophages are known to regulate endothelial germination and angiogenesis by secreting matrix metalloproteinases (MMPs) that degrade different extracellular matrix (ECM) proteins, leading to the release of pro-angiogenic growth factors into the perivascular matrix [8,9]. MMPs are zinc-dependent endopeptidases that play a key role in the imbalance between ECM deposition and degradation. Therefore, it was initially thought that MMPs may limit pulmonary fibrosis by degrading ECM proteins in the lung. However, recent studies have shown that MMPs are involved in regulating various other cellular and signaling pathways in addition to ECM proteins [10], including inflammatory mediators, growth factors, etc. [11]. Tissue fibrosis is traditionally considered to be characterized by a pathological imbalance in ECM metabolism that is irreversible. Thickened alveolar interstitial spaces with distorted epithelial and vascular structures form a unique ECM-ecological niche [12,13] that affects the proliferation, migration, and differentiation of resident cells within the lung, thus emphasizing the importance of ECM-cell crosstalk [14-16]. Most previous studies have been limited to the role of MMPs in tissue remodeling, while fewer studies have reported whether MMPs can act as a key molecule in ECM-cell crosstalk, which could influence the biological process of fibrosis. Consequently, we sought to examine the role and mechanism of ECM-cell crosstalk, including a potential role for MMPs in silicosis.

2. Materials and methods

2.1. Establishment of a mouse model of silicosis

Specific pathogen free grade male C57BL mice were utilized in experiments at 6–8 weeks of age and about 30 g. The mice were housed in a 20–22 °C room with a relative humidity of 40–60% and 12 h of light that alternated between day and night. The tracheas of the mice were exposed after intraperitoneal sodium pentobarbital anesthesia, and a single intratracheal injection of silica suspension (0.2 g/kg, 50 mg/ml saline) was given. Equal volumes of sterile saline were administered to the control group. At 7 days and 56 days after modeling, lung tissues were collected. Phosphate-buffered saline (PBS) perfusion, 4% formalin treatment, and 30% sucrose for dehydration, sectioning, and freeze staining were administered prior to immunohistochemical analysis. All animal experiments were carried out strictly in compliance with the Animal Research In Vivo Experimental Report (ARRIVE) and according to the Southeast University Laboratory Animal Center's animal management guidelines.

2.2. Single-cell RNA sequencing

2.2.1. Sample collection

Lung samples for scRNA-seq were collected from four groups of mouse whole lung tissues (NS-7d, SiO_2-7d, NS-56d and SiO_2-56d) and washed three times rapidly with precooled × *PBS.

2.2.2. Cell capture and cDNA synthesis

Lung tissue was cut into approximately 1 mm^2 pieces, and individual cells were obtained using the Lung Isolation Kit (Miltenyi Biotech, 130–095–927, Germany) and suspended in PBS containing 0.04% BSA, according to the operating protocol instructions. The captured cells (approximately 1 $\times 10^4$) were placed in individual GEMs for reverse transcription to obtain barcode codes. Reverse transcription was performed on an S1000TM Touch Thermal Cycler (Bio-Rad) (53 °C, 45 min; 85 °C, 5 min; stored at 4 °C) to obtain cDNA. Finally, the quality was assessed using an Agilent 4200 system (Beijing BIO Biotechnology Co.).

2.2.3. scRNA-seq library preparation

The scRNA-seq libraries were constructed using the Single-Cell 5′ Library and Gel Bead Kit, Single Cell V(D)J Enrichment Kit, and Human T Cell (1000005) and Single Cell V(D)J Enrichment Kit according to the manufacturers' instructions. The sequencing was performed on an Illumina NovaSeq6000 sequencer and required a depth of no less than 100,000 reads per spot, accompanied by a 150-bp paired end (PE150). Sequencing was performed by Beijing BIO Biotechnology Co.

2.2.4. scRNA-seq data pre-processing and analysis

Cell barcode filtering, comparison and UMI counting were performed using Cell Ranger 4.0.0 (https://www.10xgenomics.com/). Further analysis was conducted with the R package Seurat v3.2.2 and was based primarily on the official tutorial [17]. The double linkage rate (the nExp parameter in DoubletFinder) was estimated from the user guide for 10 × Chromium. For quality control and filtering, the R package DoubletFinder was used to detect and remove doublets [18]; cells with detected genes less than 500 or with mitochondrial gene content > 20% were excluded, and genes presented in less than 10 cells were deleted. The scRNA-seq data were normalized using Log Normalize (scale factor 10,000), two thousand highly variable genes were identified, and normalized counts were scaled by default. We performed principal component

analysis (PCA) for primary dimensionality reduction with 30 dimensions, which were selected based on the elbow plot. Batch effects among four samples were alleviated with Harmony [19]. Thirty-three Clusters were identified by the FindNeighbors (based on KNN graphs) and FindClusters (based on Louvain method, resolution = 1) functions in Seurat. Harmony embeddings were used as the input for t-distributed stochastic neighbor embedding (t-SNE) [Journal of Machine Learning Research 9 (2008) 2579–2605], which allows data visualization in a two-dimensional space. Cell-type annotation was conducted with the manually curated cell type markers and 33 clusters were merged into 20 cell types. Harmonic embeddings were used as input to t-SNE, which allows for data visualisation in two dimensions. The differential expression levels of genes were calculated using the FindMarkers, which is based on the Wilcoxon ranking and test with default parameters.

2.3. Spatial transcriptome sequencing

2.3.1. Sample collection

Mice with significant fibrotic lesions on CT imaging were selected, and their lung tissue was trimmed horizontally close to the hilum. The samples were immediately frozen in optimal cutting temperature compound on dry ice and stored at − 80 °C.

2.3.2. Staining and imaging

The 10-μm frozen sections of lung tissue were mounted on a GEX matrix, which were then placed on a thermocycling adapter with the active surface facing upwards. After incubation at 37 °C for 1 min, the sections were fixed in methanol at − 20 °C for 30 min and then H&E-stained to observe the moulding. Imaging was performed at 10 × resolution using a Leica DMI8 full-load broken section scanner.

2.3.3. Permeabilization and reverse transcription

Leak-proof grooves were constructed using a slide cassette. According to the instructions of the Visium Spatial Gene Expression Tablets and Kit (10 × Genomics, PN-1000184), 70 μl of permease was added to each groove, and the samples were incubated at 37 °C for 30 min. Next, 100 μl of SSC and 75 μl of RT Master Mix were added for cDNA synthesis (65 °C, 15 min, stored at 4 °C).

2.3.4. cDNA library preparation for sequencing

After first strand synthesis, the RT Master Mix was removed, and 75 μl of 0.08 M KOH were added. The samples were incubated at room temperature for 5 min, after which the KOH was removed, the samples were washed with 100 μl EB buffer, and Second Strand Mix (75 μl) was added to each well. After second strand synthesis, cDNA amplification was performed (98 °C, 3 min; 98 °C, 15 s; 63 °C, 20 s; 72 °C, 1 min; cycle 14 times, 72 °C, 1 min; stored at 4 °C). Visium spatial libraries were constructed using the Visium Spatial Library Construction Kit (10x Genomics, PN-1000184). The libraries were sequenced using an Illumina NovaSeq6000 sequencer with a depth of no less than 100,000 reads per spot, accompanied by a 150-bp paired end (PE150). Sequencing was performed by Beijing Brio Biotechnology Co.

2.3.5. Data preprocessing

Each point of the mouse reference genome was processed, compared and summarised with Unique Molecular Identifier (UMI) counts using 10X Space Ranger software LOL to obtain a characteristic barcode matrix. Points that covered the tissue sections were further analysed, and clustering algorithms based on 10 principal component maps were used to visualise the points in two dimensions using the t-SNE method. The final spatial transcript expression map was generated using the R package Seurat v3.2.2 [17].

2.4. Cell culture

Mouse macrophages (RAW264.7), human myeloid leukemia monocytes (THP-1), and human umbilical vein endothelial cells (HUVECs) were purchased from ATCC. Mouse lung primary endothelial cells were isolated from 7-day-old mouse lungs and verified by FACS analysis, kindly performed by Dr Qiu's Lab (Front Immunol.2021 Dec 8;12:759176). THP-1 cells were cultured in RPMI1640 containing 10% FBS, streptomycin (100 μg/ml), and penicillin (100 U/m L) in a cell culture incubator with 5% CO_2 at 37 °C, followed by stimulation of differentiation with 50 nM/well of Phorbol acetate (PMA) for 24 h. HUVECs were grown in DMEM with 10% FBS, 1% glutamine, and 1% double antibodies in an incubator at 37 °C with 5% CO_2. The cells were cultivated for passaging and amplification at 2–3-day intervals. Before being processed, the cells were injected in 24-well plates at a concentration of 1×10^5 cells/ml for 24 h. The cell concentration was adjusted according to the specific experimental requirements. Primary lung endothelial cells were cultivated in ECM medium containing 20% FBS, 1% glutamine, 1% double antibodies, and 1% Endothelial Cell Growth Supplement and were utilized for research from 3 to 5 generations at a density of less than 3×10^5 cells/ml.

2.5. Reagents

Silicon dioxide (SiO_2) pellets were purchased from Sigma-Aldrich supplied (S5631; Billerica, MA, USA), and at least 80% had a diameter of 1–5 μm. The pellets were produced using sedimentation selection, acid hydrolysis, and overnight baking (200 °C, at least 16 h) with sorting using Stokes' law. Silica samples were dissolved in saline before being used experimentally. Recombinant MMP12 protein (10266) was obtained from Yiqiao Shenzhou. MMP408 (a specific inhibitor of MMP12) was purchased from Sigma (44291). TJP1 (rabbit polyclonal antibody, 21773–1-AP), MMP12 (rabbit polyclonal antibody, 22989–1-AP), and occludin (rabbit polyclonal antibody, 13049–1-AP) were acquired from Proteintech. CDH5 (rabbit polyclonal antibody, AF3265) was purchased from Affinity.

2.6. Tube-formation assays

Ibidi angiogenesis slides were first filled with 10 μl of regular Matrigel gel per well, then placed in a moist box at 37 °C for half an hour to solidify. HUVECs were digested and resuspended in a cell suspension containing 3.0×10^5 cells/ml. The solidified gel ibidi angiogenesis slides were taken from the wet box, and 50 μl of cell suspension was added to each well. Images were captured at regular intervals (3–24 h) based on the development rate. The tube-forming length, area covered, number of loops, and number of nodes were measured and recorded. ImageJ was used for statistical analysis.

2.7. siRNA-mediated knockdown

siRNAs were purchased from Shanghai Jima Pharmaceutical Co. Ltd., and the transfection reagent Lipofectamine 3000 was purchased from Thermo Fisher Scientific. To knock down MMP12 in macrophages, 9 μl of serum-free medium and 1 μl of transfection reagent were placed in one tube, while 1.5 μl of siRNA and 9 μl of serum-free medium were placed in another tube. The solutions were incubated for 5 min at room temperature. The two solutions were then mixed and incubated for 20 min 100 μl of cell suspension containing 3×10^5 cells/ml was added to the mixture with an additional 80 μl of serum-free medium. Finally, 200 μl of the transfected cells were inoculated into the wells of a 24-well plate, and the standard medium was replaced after 24 h of incubation.

2.8. Identification of trans-monolayer cell permeability and resistance values

The measurement method was derived from previous studies with some modifications [20-22]. TEER measurements were used to estimate the integrity of cellular tight junctions by measuring the cell layer's

resistance. 3×10^5 HUVEC cells per well were cultivated on 12 mm Transwell® plates for three days to achieve 90% cell fusion. After being exposed to stimuli, Millipore Milli cell ERS-2 was used to evaluate transendothelial electrical resistance (TEER), which was calculated as follows:

$$\text{TEER } (\Omega \cdot \text{cm}^2) = (R_S(\Omega) - (R_B(\Omega) \cdot A(\text{cm}^2)$$

where R_S is the total resistance of the cell monolayer across the membrane, R_B is the blanking resistance of the blanking chamber (no cells), and A is the bottom area of the chamber (1.12 cm^2).

In FITC-dextran permeability assays, FITC-dextran (Sigma-Aldrich, relative molecular mass 40 kDa) was added to the inner chamber. After 1 h of incubation in the dark, fluorescence values were measured using an enzyme marker at 490 nm excitation and 520 nm emission wavelength (BioTek, USA). The following equation was used to determine the permeation value:

Permeation value/% = outer chamber medium FITC-dextran fluorescence value / (inner chamber medium FITC-dextran fluorescence value + outer chamber medium FITC-dextran fluorescence value) × 100%.

2.9. Cell migration assays

The cell migratory capability was measured using a wound healing test. HUVEC-GFP cells were seeded in 24-well plates at a density of 1×10^5 cells per well and incubated at 37 °C until the cells were 90% fused. Then, a medium-width straight line was scored vertically in the middle of the 24-well plate using a sterile 200-μl pipet. The plates were washed three times with PBS to remove cell debris before adding new standard media to each well to promote cell development. The cells were stimulated experimentally, and digital photographs of the scratch gaps were obtained at 0, 6, 12, and 24 h. The distances between the cell gaps were quantified using ImageJ.

2.10. Western blot assays

Western blotting was used to measure the amounts of selected proteins in THP-1 macrophages. The cells were rapidly washed with phosphate buffer and lysed to get total proteins. Protein concentrations of lysis products were determined using a BCA Protein Quantitative Kit (Beyotime, China), then separated using SDS-PAGE gel electrophoresis and transferred to PVDF membranes. After blocking, the membranes were treated with primary antibodies overnight at 4 °C. After washing with TBST, they were incubated for 1 h at room temperature with horseradish peroxidase-labeled secondary antibodies. The chemiluminescence detection technique was used to reveal protein bands, and ImageJ was used to quantify the protein. All Western blotting tests were performed at least three times.

2.11. Immunofluorescence staining assays

The lung tissues or ECM were sliced into 8-m slices and placed in a freezing microtome. The sections were treated with specific primary antibodies at 4 °C overnight after being sealed with 10% goat serum in 0.3% Triton X-100 for two hours at room temperature. The next day, nuclei were stained with DAPI by incubating them for two hours with a suitable fluorescent secondary antibody at room temperature (Alexa Fluor, Thermo Fisher Science). The FV3000 was used to capture the images.

2.12. Real-time quantitative RT-PCR assays

The relative expression of *Mmp12* mRNAs was determined using real-time quantitative RT-PCR (qRT-PCR). THP-1 cells were inoculated at the density required for the experiment, induced into macrophages with PMA, and treated accordingly after 24 h. The cells were washed three times with ribonuclease-free PBS, and total RNA was extracted using TRIzol reagent (Invitrogen) according to the manufacturer's instructions. The concentration of the RNA was determined using a NanoDrop One spectrophotometer (Thermo Fisher Science). The RNA were normalized to include 400 ng of RNA and reverse transcribed into cDNA, which was utilized as a template for quantitative reverse transcription polymerase chain reaction. The cell cycle threshold (Ct) and the Ct value were determined, and quantification was carried out utilizing Opticon monitoring software (Bio-Rad). The relative mRNA expression measurement was adjusted to an endogenous reference (*Gapdh*).

2.13. Decellularisation of the lung matrices

Lung tissue slices were frozen at − 80 °C and then frozen tissue sections of 200 μm were made on a frozen sectioning machine. The tissue sections were sequentially placed in lysis buffer (1% SDS in ddH_2O), 1% Triton X-100 (diluted with ddH2O) and NaCl (1 M) for decellularisation at room temperature. Tissue sections were then treated in a solution containing DNase (20 μg/ml) and MgCl (4.2 mM) in a mixture of solutions and incubated for 1 h at 37 °C. The decellularisation process was terminated after aspiration of DNase.

2.14. Statistical analysis

Statistical analysis was performed using GraphPad Prism 8.0.2 (GraphPad Software, USA). Two-group comparisons were assessed for significance using the two-tailed Student's t-test. Multiple group (three or more group) comparisons were performed using one- and two-way ANOVA. All data are expressed as the mean ± SEM, and differences were considered statistically significant when $P < 0.05$.

3. Results

3.1. Aberrant interactions between macrophage and endothelial cells are observed in the mouse silicosis model

To explore mechanisms of crosstalk between macrophages and endothelial cells during silicosis progression, we employed a mouse silicosis model. After 56 days of suspension infusion, H&E staining (Fig. 1A) revealed that the alveolar structure of the mice from the silica group (SiO_2) was disturbed, with hemorrhagic patches and enlarged alveolar septa relative to the lungs of the control (NS) group. The gross lung tissue in the silica group demonstrated an increase in lung volume together with edema and blood exudation, with high-density shadows in CT scans after 56 days, indicating a serious insult to the lung tissue with a compromised endothelial cell barrier function (Fig. 1B). To evaluate changes in the cellular composition of the lung tissue after SiO_2 exposure, we performed single cell RNA sequencing (scRNA-Seq) on lung tissue samples. A total of 20 clusters were identified, which were viewed in two dimensions using t-SNE[23]. Although the number of endothelial cells did not change considerably, the number of macrophages was significantly higher in the silica group than in the control group (Fig. S1C). Interestingly, endothelial cells in the silica group showed decreased mRNA expression levels of the tight junction protein *tjp1* and the calmodulin *cdh5* (Fig. 1C), suggestive of reduced barrier function. The effect of SiO_2 in compromising the alveolar barrier was further verified by the reduced expression of the endothelial barrier protein occludin (Fig. 1D).

To investigate the interactions between endothelial cells and macrophages in lung tissue, we used the CellChat database of ligand-receptor interaction pairings created by Efremova et al. [24]. Potential linkages between macrophages, endothelial cells, epithelial cells, and stromal cells were identified in terms of the type, quantity, and strength of reciprocal receptor-ligand interactions. The results show that in the

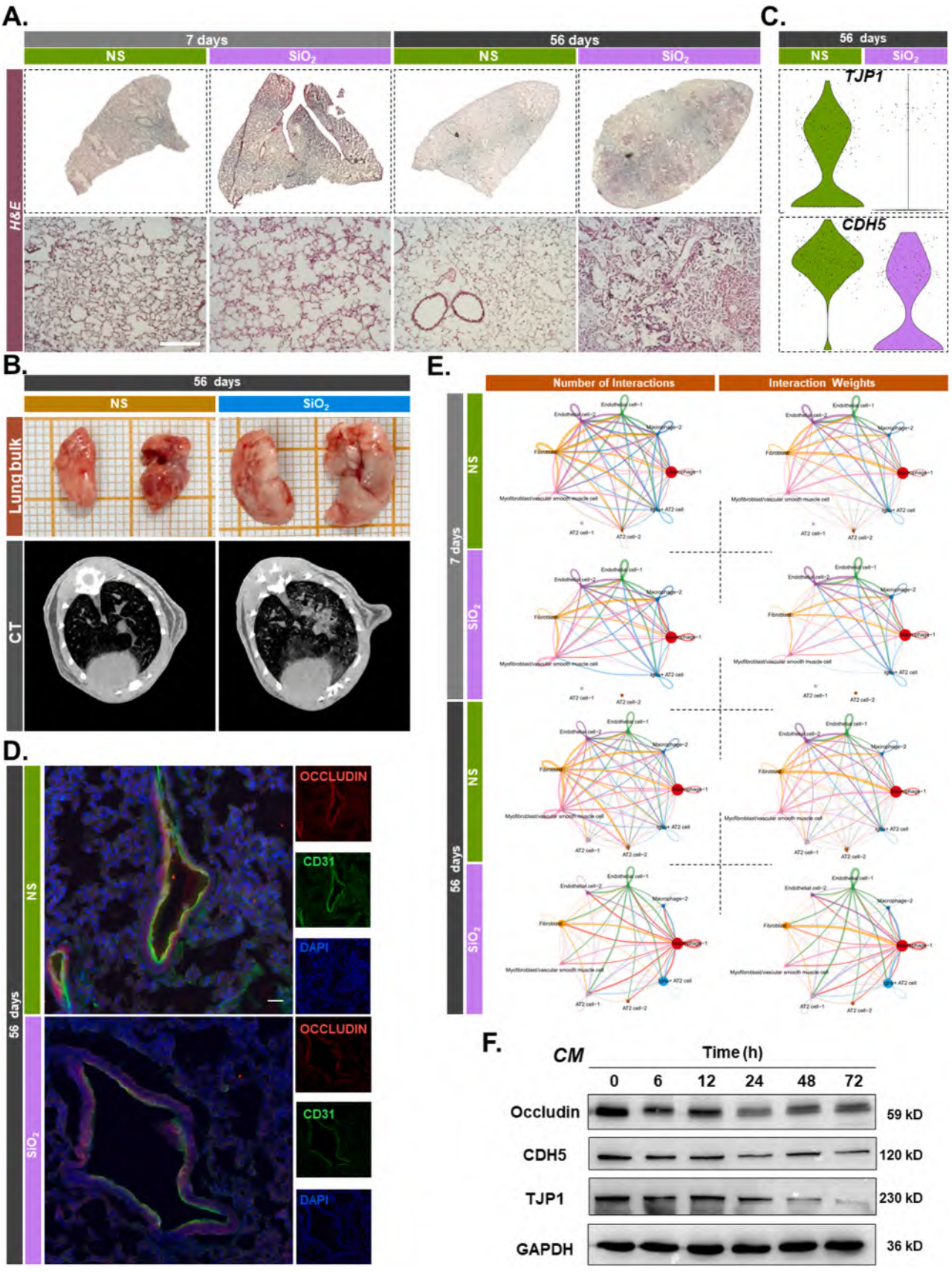

(caption on next page)

Fig. 1. Single-cell sequencing analysis of macrophage and endothelial cell interactions. (A) H&E staining of lung tissues from control saline-treated mice (NS) and silica-treated mice (SiO_2) after 7 or 56 days of treatment. Mice in the silica group had higher collagen deposition than mice in the saline group, suggesting effective modeling. Scale bar= 200 μm. (B) Gross and CT scan images of the lungs. Compared to the control group, mice exposed to silica dust exhibited expanded lung tissue and high-density lung tissue shadows. (C) Expression of *tjp1* and *cdh5* in endothelial cells. (D) Immunofluorescence staining of the endothelial cell marker CD31 and the tight junction protein occludin in mouse lung tissues. Scale bar = 20 μm. (E) Network of interactions predicted in silica dust-treated lungs. The nodes represent clusters and edges represent the number of meaningful ligand-receptor pairings. (F) Representative western blot showing that conditioned medium of macrophages treated with SiO_2 (CM) resulted in decreased expression of tight junction proteins occludin and TJP1 and calmodulin CDH5 in HUVECs, n = 5, $P < 0.05$ compared to the 0 h group.

control group, interactions with endothelial-1 cells, compared to other intrinsic cells (including endothelial-2 cells, fibroblasts, myofibroblasts, and epithelial cells), were strongest for macrophage-1 cells on day 7 and macrophage-2 cells on day 56 (Fig. S1A). This is consistent with the possibility that macrophage-endothelial-1 interactions may maintain the balance of typical lung biological activities under physiological circumstances. We further examined the connections between macrophages and endothelial cells after silica treatment. In the silica group compared to the control group, the number of possible ligand-receptor and ligand-receptor strength interactions between macrophages and endothelial cells showed a predominate trend of reduction (Fig. 1E and S1B, C). To mimic a silica-stimulated intrapulmonary inflammatory milieu, we co-cultured alveolar macrophage conditioned cultures treated with SiO_2 (CM) with endothelial cells. Over time, the expression of CDH5, TJP1, and Occludin protein was reduced (Fig. 1F and S1D–F). In addition, analysis of cell-cell interactions by Transwell experiments (Figs. S2A-F) further supports the possibility that aberrant macrophage-epithelial interactions may mediate endothelial cell injury in response to SiO_2 stimulation.

3.2. Key molecules underlie endothelial cell functional alterations in macrophages

To explore the mechanisms of endothelial cell injury in our silicosis model, we evaluated the roles of the top 100 genes of macrophages and endothelial cells from the above scRNA-Seq; these genes intersected in the "regulation of cytokine production" and "regulation of cell adhesion" pathways (Fig. 2A–C). Genes enriched in the above two pathways were further evaluated by intersection analysis with the top 20 genes of macrophages (Fig. S3A, B), suggesting key roles for four intersecting genes (MMP12, CCL2, GPNMB, and Il-1β; see Fig. 2D). Protein network interaction analysis (PPI) of these four genes with the genes related to endothelial cell function revealed that three of them (MMP12, CCL2, and Il-1β) functionally interacted with genes expressed in endothelial (Fig. S3C). Based on five classification techniques (MNC, DMHC, Radiality, Closeness, and Stress) in the cytoHubba plugin, the top 20 genes for each ranking method were chosen in the Cytoscape program. Finally, by considering the top 20 genes in the Wayne diagram, the top core gene, *Mmp12*, was filtered (Fig. 2E).

To provide additional evidence for the key role of *Mmp12*, we evaluated its expression as compared to the expression of other MMP family members. The results confirmed that *Mmp12* displayed differential expression when adjusted to create normalized standard values and coupled with differential expression ploidy log|2 FC= and q-value (Fig. S3D, E). Additionally, assessment of the GEO clinical database revealed that *Mmp12* expression was higher in patients' lungs with idiopathic pulmonary fibrosis (IPF) than in healthy controls (Fig. S3F). scRNA-Seq revealed that *Mmp12* expression levels were higher in macrophages from the silica group than from the control group of mice (Fig. 2F, G). Furthermore, macrophages tended to collect in areas of inflammation and nodular lesions (Fig. 2H). Immunofluorescence staining (Fig. 2I), further verified that *Mmp12* in macrophages is increased in response to SiO_2 stimulation, thus supporting its potential role in silicosis.

3.3. Increased MMP12 expression is associated with M1 macrophage activation after SiO_2 treatment

To investigate which cell subtypes are responsible for changes in endothelial cell function after SiO_2 treatment, we divided macrophages according to cell markers, into M1, M2, and S100a9^{high} subtypes (Fig. 3A, B). The number of M1 macrophages (Fig. 3C) and the expression of IL-1β and TNF-α, both markers of M1 activation (Fig. S4A–C), were higher in the silica group than in the saline group. Based on the three subpopulations of macrophages, *Mmp12* was found to show differential expression only in M1, and the expression was greater in the silica group than in the control group on the 7th and 56th days (Fig. 3D, E). For additional verification, we treated resting-state macrophages (PMA-induced THP-1 cells) with SiO_2 suspension, which revealed a time-dependent increase in MMP12 expression (Fig. 3F and S5A). Similar results were observed for Raw 264.7 murine-derived macrophages (Fig. S5B, C). NOS2 (a marker of M1 macrophages) and ARG1 and SOCS3 (markers of M2 macrophages) expression levels were also considerably enhanced (Fig. 3G and S5D–F). Furthermore, when lipopolysaccharide (LPS) was utilized to convert resting macrophages to an activated M1 state, subsequent treatment with SiO_2 revealed a comparable time-dependent rise in MMP12 expression (Fig. 3H and S5G). These results suggest that MMP12 expression is enhanced with SiO_2 treatment in M1 macrophages.

3.4. Macrophage-derived MMP12 is involved in endothelial cell dysfunction

To investigate whether MMP12 regulates the altered endothelial cell vascular function associated with silicosis, we performed PPI analysis focused on MMP12. The findings reveal interactions between MMP12 and TJP1, CDH5, and Occludin (Fig. 4A). Furthermore, GO analysis of differentially expressed genes in macrophages revealed that MMP12 is enriched in biological processes that regulate blood vessels (Fig. 4B). To further investigate the relationship between changes in MMP12 protein in macrophages and endothelial cell function, we treated HUVECs for 48 h with recombinant MMP12 (rhMMP12). Western blotting assays revealed that the expression of occludin, CDH5, and TJP1 in HUVECs was significantly reduced by rhMMP12 (Fig. 4C and S6A–G). Furthermore, in scratch test and tube formation assays of endothelial vascular cell function, the addition of rhMMP12 substantially reduced the HUVEC migratory ability (Fig. 4D, E), hindered tube formation (Fig. 4F, G), and increased permeability (Fig. 4H, I).

To further verify that macrophage-derived MMP12 is involved in endothelial cell injury, we cultured *Mmp12* knockdown macrophages with and without SiO_2 treatment, prior to culture of HUVECs in the resulting conditioned medium (CM) (Fig. 5A and S6H, I). The reduction in Occludin, CDH5, and TJP1 expression caused by SiO_2-treated macrophage CM was considerably reversed by knockdown of *Mmp12* (Fig. 5B and S6J–L). At the same time, *Mmp12* knockdown in CM prevented tube formation, reduced resistance values, and reversed the increase in permeability caused by SiO_2-treated conditioned cultures (Fig. 5C–F).

3.5. Macrophage-derived MMP12 partially accumulates in the ECM

To further explore the role of MMP12 in SiO_2-dependent macrophage

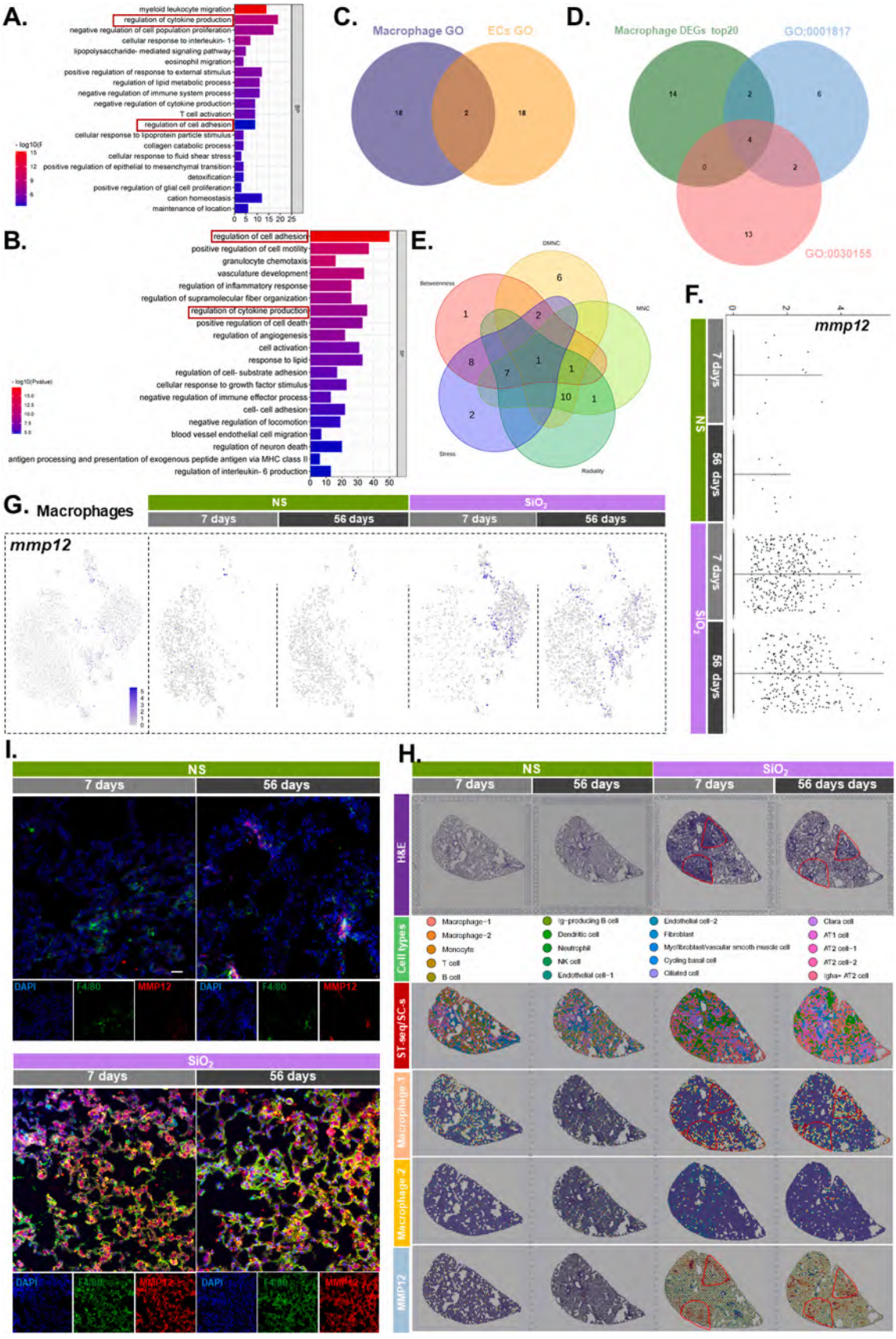

(caption on next page)

Fig. 2. Screening for key molecules involved in endothelial cell function alterations by macrophages. (A, B). GO enrichment analysis of the top 100 differentially expressed genes in macrophages (panel A) and endothelial cells (panel B) from lungs of SiO_2 versus control (NS) mice at 56 days. (C) Venn diagram showing the overlap between endothelial and macrophage top100 gene biological processes. (D) Venn diagram showing the top 20 genes in macrophages that are enriched for the gene ontology pathways "regulation of cytokine production" (GO:0001817) and "regulation of cell adhesion" (GO:0030155). (E) The top 20 genes from differentially expressed genes of macrophages were categorized by the cytoHubba five techniques (DMNC, MNC, Radiality, Stress, Betweenness). (F) Violin graphs showing the levels of the total macrophage *mmp12* mRNA expression in the silica dust and control saline groups. (G) t-SNE plot illustrating changes in the levels of *mmp12* mRNA expression in M1 from the silica and control groups. (H) Single-cell spatial transcriptome mapping and the spatial expression of *mmp12* mRNA. (I) Immunofluorescence staining of mouse lung tissue slices to detect co-localized expression of the macrophage markers F4/80 with MMP12. Scale bar= 20 μm.

function, GO analysis of differentially expressed genes in macrophages was performed, which suggested that the MMP12 protein is enriched in the ECM (Fig. 6A). Because abnormal accumulation of ECM during silicofibrosis has been reported to affect resident cells in the lung [13], we sought to determine the ECM protein changes in pulmonary fibrosis samples. Lung tissue ECM proteins were extracted from the control and silica groups of mice for proteomic analysis, and MMP12 was identified as a differentially expressed protein using $|Log2FC= \geq 1, P < 0.05$ as the screening criterion (Fig. S7A) [23]. Heat mapping based on normalized expression values of the MMP family revealed that MMP12 was most highly differentially regulated (Fig. 6B). Furthermore, both western blotting and immunofluorescence staining results showed increased levels of MMP12 protein in pulmonary fibrosis-like ECM (Fig. 6C, D). To verify whether the MMP12 accumulation in ECM may be derived from macrophages, RAW264.7 cells were first transplanted onto decellularized ECM of normal mice and cultured for 3 days after stimulation with a SiO_2 suspension. Immunofluorescence staining showed that MMP12 was detectable in the ECM, and that the expression of MMP12 was higher after SiO_2 stimulation (Fig. 6E). To distinguish whether the detected MMP12 was accumulated in ECM rather than being representative of intracellular MMP12, a portion of the samples were decellularized prior to immunofluorescence staining. However, MMP12 did not disappear with decellularization, suggesting that macrophages secrete MMP12 and partially accumulate in the ECM in response to SiO_2 stimulation (Fig. 6E, second row).

To further investigate the connection between macrophages, MMP12, and lung ECM, we injected disodium chlorophosphate liposomes (100 μl at 5 mg/ml) into the tail veins of silicosis model mice to eliminate macrophages (Fig. 7A). H&E and Masson staining showed structural disorganization of the ECM and excessive collagen deposition in silicosis mice compared with control mice (Fig. S7B). Furthermore, lung CT scans of the mice showed a decrease in the dense mass shadows in both lungs after macrophage removal (Fig. S7C, first row). After decellularization, ECM, H&E and Masson staining showed that the lung ECM of silicosis mice was less disorganized and collagen deposition was reduced after macrophage clearance (Fig. S7C, last three rows). To investigate the effect of macrophage clearance on MMP12 protein expression, we performed western blotting assays; a significant decrease in MMP12 levels was observed in macrophage-cleared mice (Fig. 7B). Moreover, immunofluorescence staining of mouse lung tissues showed that the expression of macrophage markers F4/80 as well as MMP12 were decreased after specific knockdown of macrophages, though co-localization was still observed (Fig. 7C). MMP12 expression was also decreased after decellularization in ECM, thus supporting the role of macrophages as a source for MMP12 (Fig. 7D). The above results suggest that the high level of MMP12 in ECM is partially derived from macrophages and that when macrophages are reduced, the MMP12 accumulated to ECM is also reduced.

3.6. *MMP12 accumulation in the ECM induces endothelial cell dysfunction*

To verify whether MMP12 accumulated in the ECM can continuously cause endothelial cell injury, we pretreated decellularized ECM with MMP408, an inhibitor of MMP12, at 10 μg/ml to further examine if MMP12 may alter endothelial cell function in lung fibrosis-like ECM. Primary lung endothelial cells were transplanted onto normal ECM and fibrosis-like ECM. The results of three-dimensional cell migration assays and CCK-8 assays show that the addition of MMP408 reversed the decrease in endothelial cell viability as well as the decrease in migration to fibrosis-like ECM (Fig. 8A–D). The above results suggest that MMP12 affects endothelial cell function via the lung ECM.

4. Discussion

As one of the most serious occupational diseases in the world, [25] silicosis has been an important focus of the public health community because of its high prevalence in developing countries [26]. The challenge in its treatment lies in both the lack of specific targets for screening and diagnosis in the early stages, and the lack of specific therapeutic measures in the later stages. The lung is a highly vascularized organ responsible for efficient gas exchange [27]. The intravascular space is covered by pulmonary endothelial cells, and because the endothelium is anatomically adjacent to both epithelial and mesenchymal cells [28], it has been proposed that it may contributes significantly to the development of pulmonary fibrosis [29-31]. Inflammatory reactions to tissue fibrosis are contributed by activated endothelial cells, which may manifest their effects by either initiating the inflammatory response or by fostering an already present response. Both routes involve endothelial cells, fibroblasts, cytokines, and inflammatory cells in a complicated network of feedback interactions [32]. Resting endothelial cells are also essential for maintaining vascular function. For example, signaling pathways modulated by resting endothelial cell-binding paracrine factors have been shown to maintain homeostasis and inhibit fibrosis [5]. Therefore, the development of silicosis is likely to involve a variety of molecular and cellular interactions.

In the current study, we found that the lung tissues of mice were larger after SiO_2 exposure, with edema and blood exudation, while the expression levels of endothelial tight junction protein (TJP1) and calmodulin (CDH5) were decreased (Fig. 9). As the major interconnecting proteins between vascular endothelial cells, these two proteins mediate the stability of endothelial junctions and related signaling, as well as regulating vascular remodeling and maintaining vascular integrity [33]. We also demonstrated that levels of the tight junction linker protein occludin were reduced, which further verifies the ability of SiO_2 to disrupt the barrier function of the endothelium. Disruption of vascular integrity is thought to be a phenotype of endothelial cell activation [33]. Activated endothelial cells contribute to tissue fibrosis in a variety of ways, often by directly or indirectly inducing an inflammatory response [34,35]. Moreover, vascular rarefaction is known to precede fibrosis, especially in kidney injury models [36,37]. Therefore, it is likely that the increase in permeability of the lung resulting from endothelial activation is a key underlying mediator of fibrotic changes associated with silicosis.

A variety of different cell types exist in the local vascular microenvironment, including specialized subgroups of immune cells, such as macrophages that can regulate the angiogenic process [38,39]. Previous studies in our laboratory have demonstrated the effect of macrophage polarization on fibrosis. We confirmed that M1 macrophages induced with SiO_2 in the early stage of silicosis initiates inflammation, followed by fibrosis mediated by M2 macrophages in the late stage of silicosis, for which autophagy plays an important role [40,41]. Moreover, the effect of SiO_2 on M1 and M2 polarization are also mediated by epigenetic mechanisms, such as circRNAs and ubiquitination [42,43]. On the other

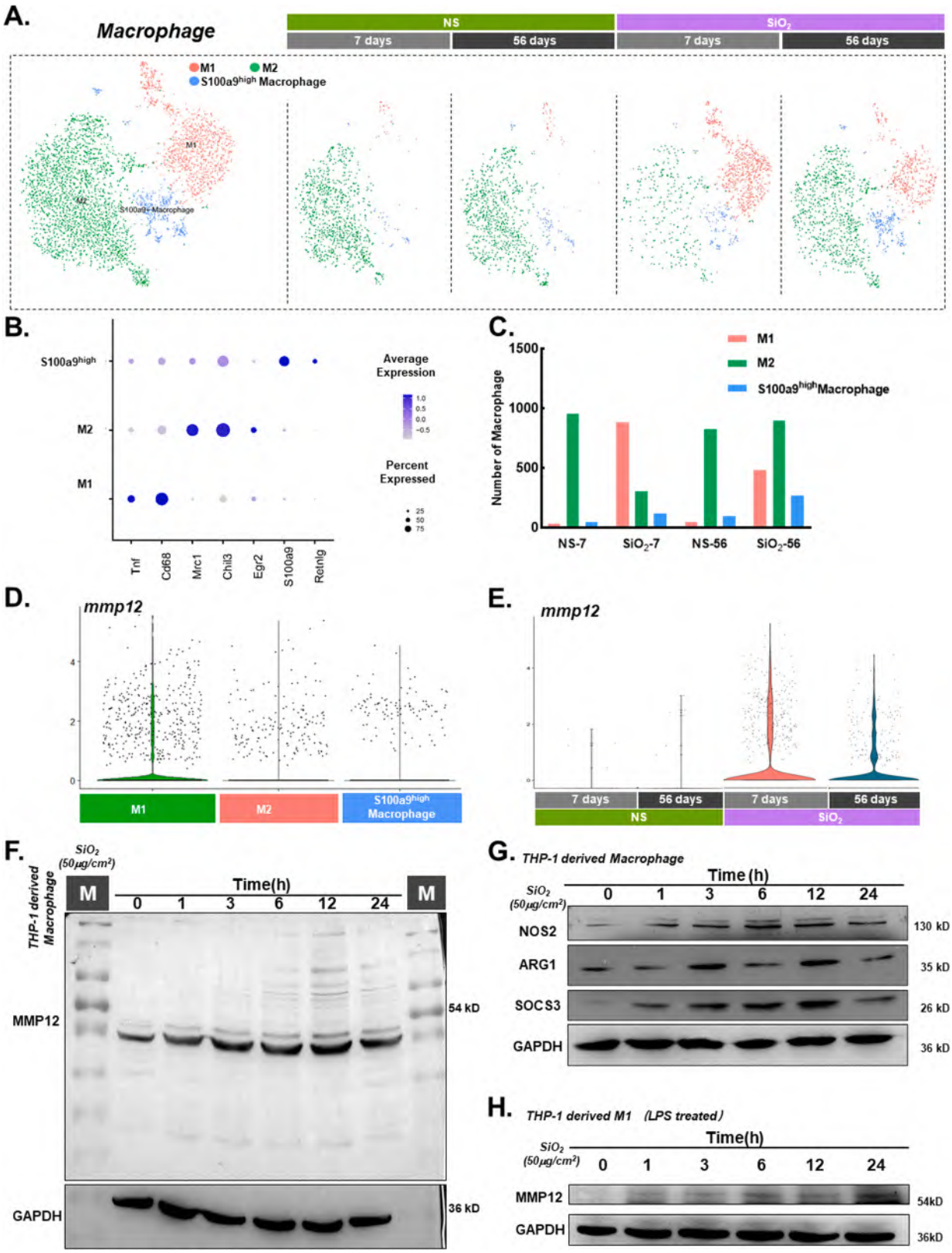

Fig. 3. SiO_2-induced macrophage activation leads to increased MMP12 expression. (A) t-SNE demonstrates three subclusters of macrophages in control (NS) and SiO_2-treated mouse lungs. (B) A bubble diagram showing macrophages divided into three subpopulations based on cellular markers, with the bubble size representing expression levels. (C) Changes in the cell numbers of macrophage subclusters in control and SiO_2-treated mouse lungs at 7 and 56 days. (D) Violin plot showing *mmp12* mRNA expression levels in three subclusters of macrophages. (E) Violin plot showing *mmp12* mRNA expression levels in M1 macrophages. (F) Representative western blotting assay to determine MMP12 protein levels in THP-1 macrophages induced into a resting state with PMA. (G) Representative western blotting assay to detect NOS2, ARG1, and SOCS3 levels in THP1 macrophages induced into a resting state with PMA. (H) Representative western blotting assay to detect MMP12 levels in THP1 cells induced into an activated M1 state with LPS.

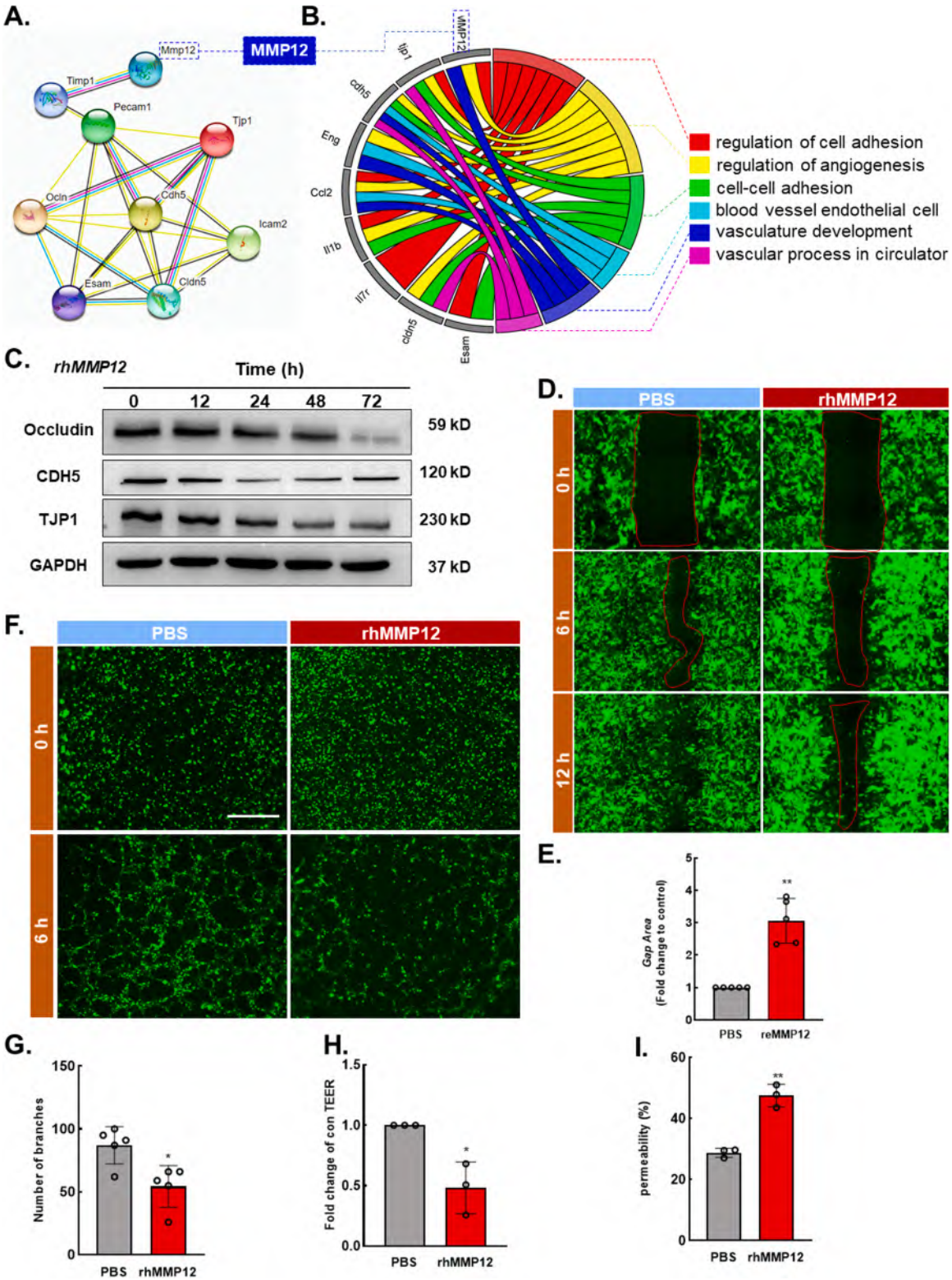

Fig. 4. MMP12 is involved in endothelial cell dysfunction. **(A)** Protein-protein interaction (PPI) analysis demonstrates the interaction of MMP12 with endothelial cell function-related proteins. (B) The GO chord diagram demonstrates the biological process of MMP12 protein enrichment in relation to endothelial cell function. (C) In HUVECs, the expression of occludin, CDH5, and TJP1 is reduced in a time-dependent manner. (D) Wound healing assay to detect changes in migration of rhMMP12-treated HUVEC cells. (E) Quantification of the results from panel D. * * $P < 0.01$ indicates diminished migratory capacity in the rhMMP12 group compared with the PBS group, n = 5. (F) Tube formation assays were used to detect the tube formation ability after rhMMP12 treatment of HUVECs. Scale bar = 650 μm. (G) Quantification of the results from panel E. * $P < 0.05$ indicates a significant decrease in tube-forming ability after rhMMP12 treatment compared with the PBS group, n = 5. (H) Transendothelial electrical resistance (TEER) values indicate the change in HUVEC resistance after rhMMP12 stimulation. * $P < 0.05$ indicates a significant decrease in resistance values in the rhMMP12 group compared with the PBS group, n = 5. (I) Permeability results showing that after rhMMP12 stimulation, the permeability of HUVEC is elevated. * * $P < 0.01$ indicates a significantly higher permeability in the rhMMP12 group compared with that in the PBS group.

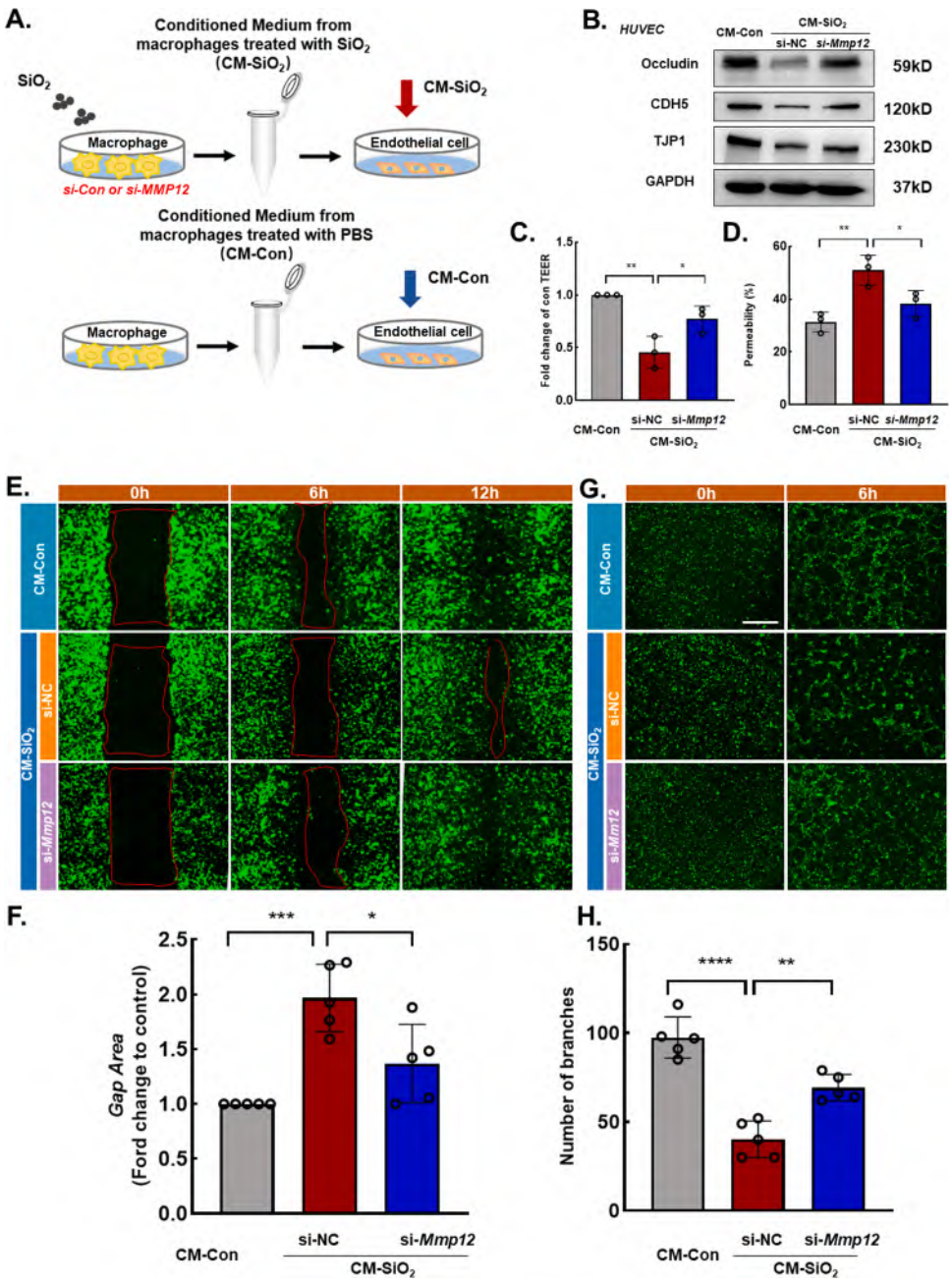

Fig. 5. Macrophage-derived MMP12 is involved in endothelial cell dysfunction. (A) The process of obtaining macrophage conditioned culture medium (CM) for co-culture with HUVEC. (B) Knockdown of *Mmp12* partially reversed the CM-SiO_2-induced decrease in the expression of occludin, CDH5 and TJP1. (C) Transendothelial electrical resistance (TEER) values show that downregulation of *Mmp12* expression reverses the CM-SiO_2-induced decrease in resistance values. * * $P < 0.01$ indicates significantly lower resistance values in the CM-SiO_2 group compared with that in the CM-Con group. * $P < 0.05$ suggests that after treatment, the si-*Mmp12* group had significantly higher resistance values than in the si-NC group. (D) Permeability results showing that downregulation of *Mmp12* expression reverses the CM-SiO_2-induced elevation in permeability. * * $P < 0.01$ indicates a significantly higher permeability in the CM-SiO_2 group compared with that in the CM-Con group. * $P < 0.05$ suggests that after treatment, the si-*Mmp12* group had a significantly lower permeability than the si-NC group.(E, F) Wound healing assay showed that downregulation of Mmp12 expression reversed the cell migration inhibited by CM-SiO_2. * ** $P < 0.001$ suggests that cell migration was significantly lower in the CM-SiO_2 group than in the CM-Con group. * $P < 0.05$ suggests that the cell migration ability of the si-*Mmp12* group was higher than that of the si-Con group after treatment. (G, H) Tubule formation assay showed that down-regulation of Mmp12 expression reversed CM-SiO_2 inhibition of the tube-forming ability. Scale bar= 650 μm. * ** * $P < 0.0001$ suggests that the cellular tube formation ability of the CM-SiO_2 group was significantly lower than that of the CM-Con group; * * $P < 0.01$ suggests that the cellular tube formation ability of the si-*Mmp12* group was higher than that of the si-Con group after treatment.

hand, SiO_2 also induces apoptosis of macrophages through the MCPIP1 pathway, which mediates the activation of fibroblasts followed by fibrosis [44]. Furthermore, the polarization of macrophage is a potential therapeutically target via treatment with neogambogic acid (NGA), which inhibits their apoptosis [45]. It would be valuable to confirm the relationship between macrophage polarization and fibrosis in patients using a clinically available macrophage polarization inhibitor in the future.

In the present study, we observed that under physiological conditions, macrophages had stronger interactions with endothelial cells than with epithelial or mesenchymal cells, and the strength of the interaction was altered in the SiO_2 group compared to the NS group, suggesting that

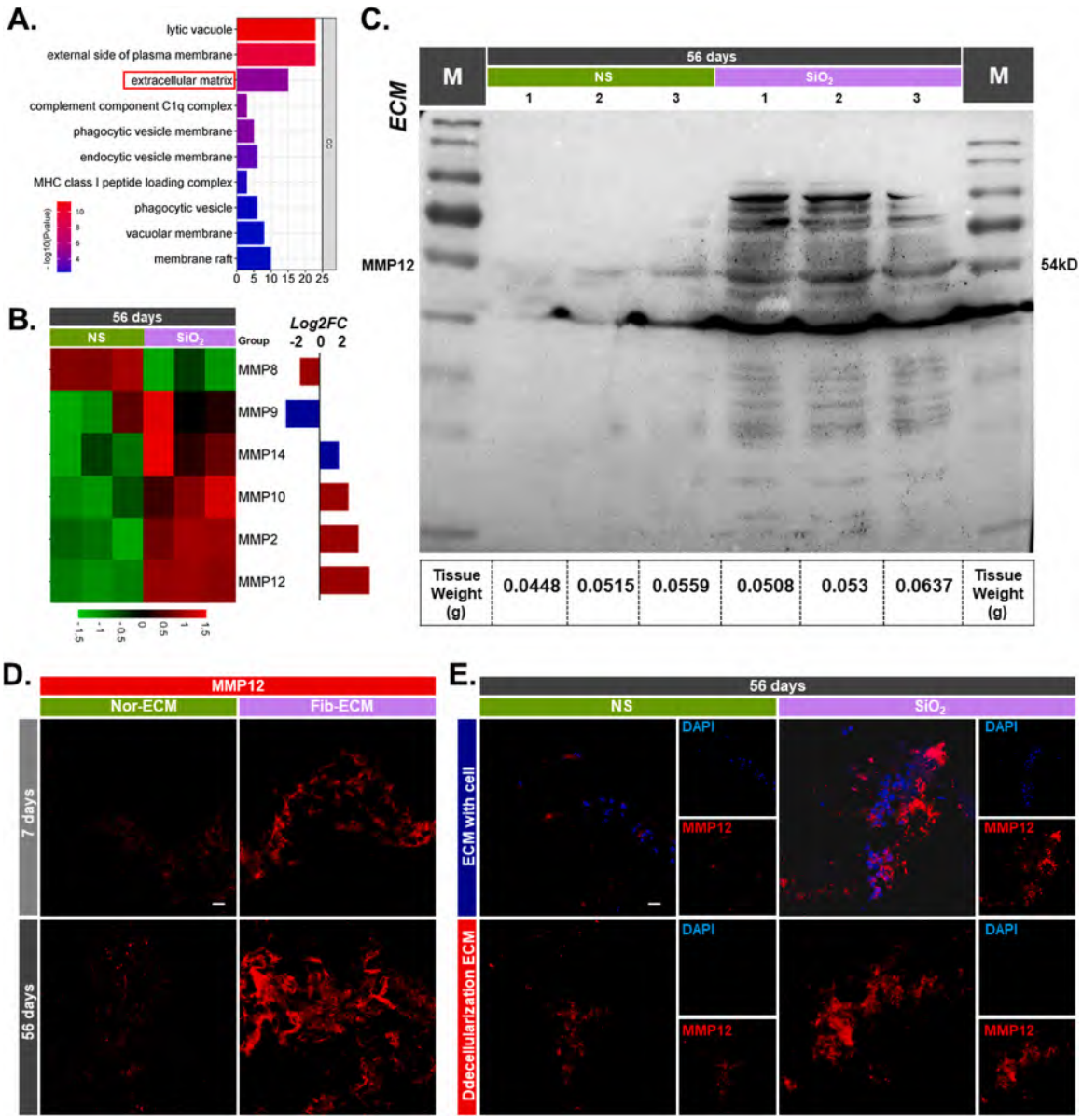

Fig. 6. MMP12 partially accumulates in the ECM. **(A)** Cellular components involved in the top 100 genes of macrophages. (B) Heat map showing the clustering of each protein of the MMP family in lung ECM proteins in lungs of control (NS) and SiO_2-treated mice. The bar chart shows the Log|2FC= values of each protein in SiO_2 mice relative to NS mice. (C) Representative western blot of MMP12 content in mouse lung ECM, n = 3. (D) Immunofluorescence staining of MMP12 in mouse lung ECM. Scale bar = 20 μm. (E) Immunofluorescence staining to detect MMP12 expression in ECM after macrophage transplantation and MMP12 accumulation in lung ECM after transplantation and decellularization treatment. Scale bar= 20 μm.

macrophage-endothelial interactions may contribute to the progression of silicosis. We therefore speculate that macrophage polarization may affect the fibrosis process by influencing endothelial cell. Growing evidence supports the role of alveolar macrophages in acute lung injury, and macrophages have also been shown to be essential for the maintenance of endothelial cell function in the physiological state [46]. After exposure to disease or injury, activated tissue-resident macrophages release inflammatory mediators (TNF-α, IL-1β, IL-6), which in turn disrupt endothelial cell-cell adhesion junctions and lead to the formation of intercellular gaps. Roy et al. [47] found that NOS1-mediated macrophage-endothelial cell interactions affect atherosclerotic progression and that macrophage-derived Wnt signaling increases endothelial permeability in a VEGF-dependent manner after muscle injury [48], while alveolar macrophages have also been reported to drive the development of lung reperfusion injury by enhancing endothelial cell production of pro-inflammatory chemokines [49]. Thus, macrophages are likely to play an important regulatory role in macrophage-endothelial cell interactions and are essential for normal embryonic development and tissue homeostasis, as well as for the immune response to invading pathogens [9].

In addition, their roles in providing protection against lung injury and infection via communication with endothelial cells, macrophages regulate endothelial germination and angiogenesis by secreting proteases that degrade different ECM proteins (including collagen, laminin and elastin) and by releasing pro-angiogenic growth factors embedded in the perivascular matrix [8,9]. MMPs are activated when their catalytic structural domain comes into contact with protein substrates and cleaves them at specific sites, destroying extracellular scaffolds or modifying bioactive molecules in the ECM [50]. Active MMP9 produced by neutrophils is associated with vascular injury and may lead to mobilization of bone marrow mesenchymal stem cells ($CD34^+$ stem cells), which contributes to reendothelialization and restenosis in

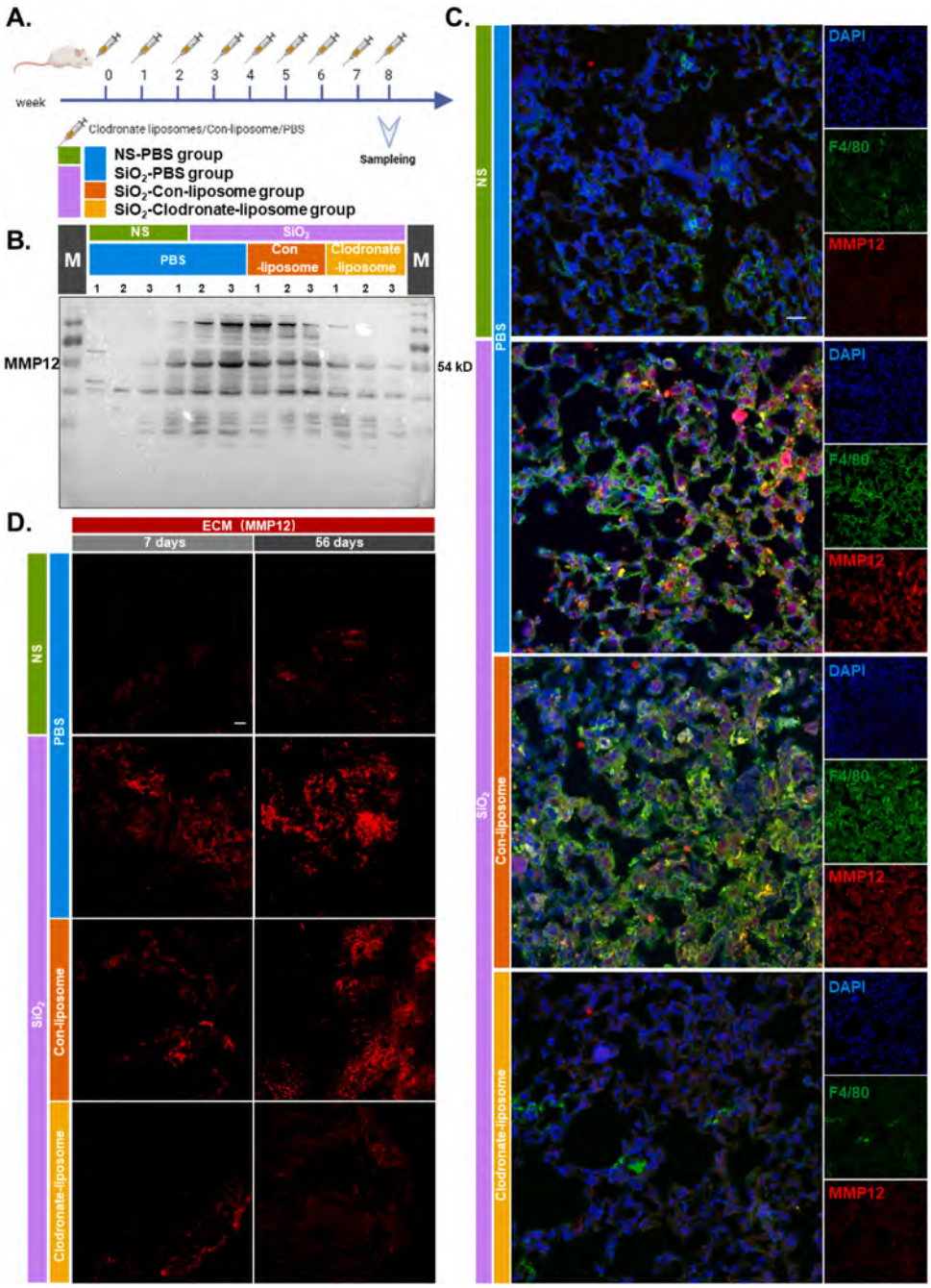

Fig. 7. MMP12 accumulation in ECM is partially derived from macrophages. **(A)** Experimental design of silicosis mice injected with disodium chlorophosphite liposomes to eliminate macrophages. (B) Representative western blot assays to analyse MMP12 content in macrophage-cleared mouse lung ECM, n = 3. (C) Immunofluorescence staining analysis of the macrophage markers F4/80 as well as MMP12 expression in lung tissue. Scale bar= 20 μm. (D) Immunofluorescence staining to detect MMP12 expression in mouse lung decellularized ECM. Scale bar= 20 μm.

patients with coronary stent implantation [51,52]. MMP2 has also been linked to normal and tumor angiogenesis, as well as the development of atherosclerosis and neointimal lesions. In our study, MMP12 was identified as a possible key macrophage molecule involved in the induction of endothelial cell injury in silicosis. MMP12 is known to be involved in many physiological processes such as embryonic development, reproduction, and tissue remodeling [53]. Furthermore, MMP12 has been implicated in the pathogenesis of inflammatory diseases such as chronic obstructive pulmonary disease, emphysema, asthma, skin diseases, arthritis, and tumors [54]. Because MMP12 levels and activity in the sputum of chronic obstructive pulmonary disease patients are directly related to the degree of emphysema, blocking MMP12 activity may prevent the worsening of the disease [55]. Patients with systemic sclerosis and interstitial lung disease also have higher levels of MMP12 in their blood and lungs, respectively, which is correlated with worsening measures of pulmonary function [56]. Therefore, our findings are consistent with the established role of MMP12 in other lung inflammatory conditions.

In previous studies, MMP12 has been shown to be protective against tumor progression [57,58], and this activity was ascribed to the generation of anti-angiogenic peptides [59]. However, in recent years, an increasing number of studies have demonstrated that MMP12 may also play a key role in fibrosis. This includes delineation of the potential value of MMP12 as a disease-related biomarker in patients with IPF

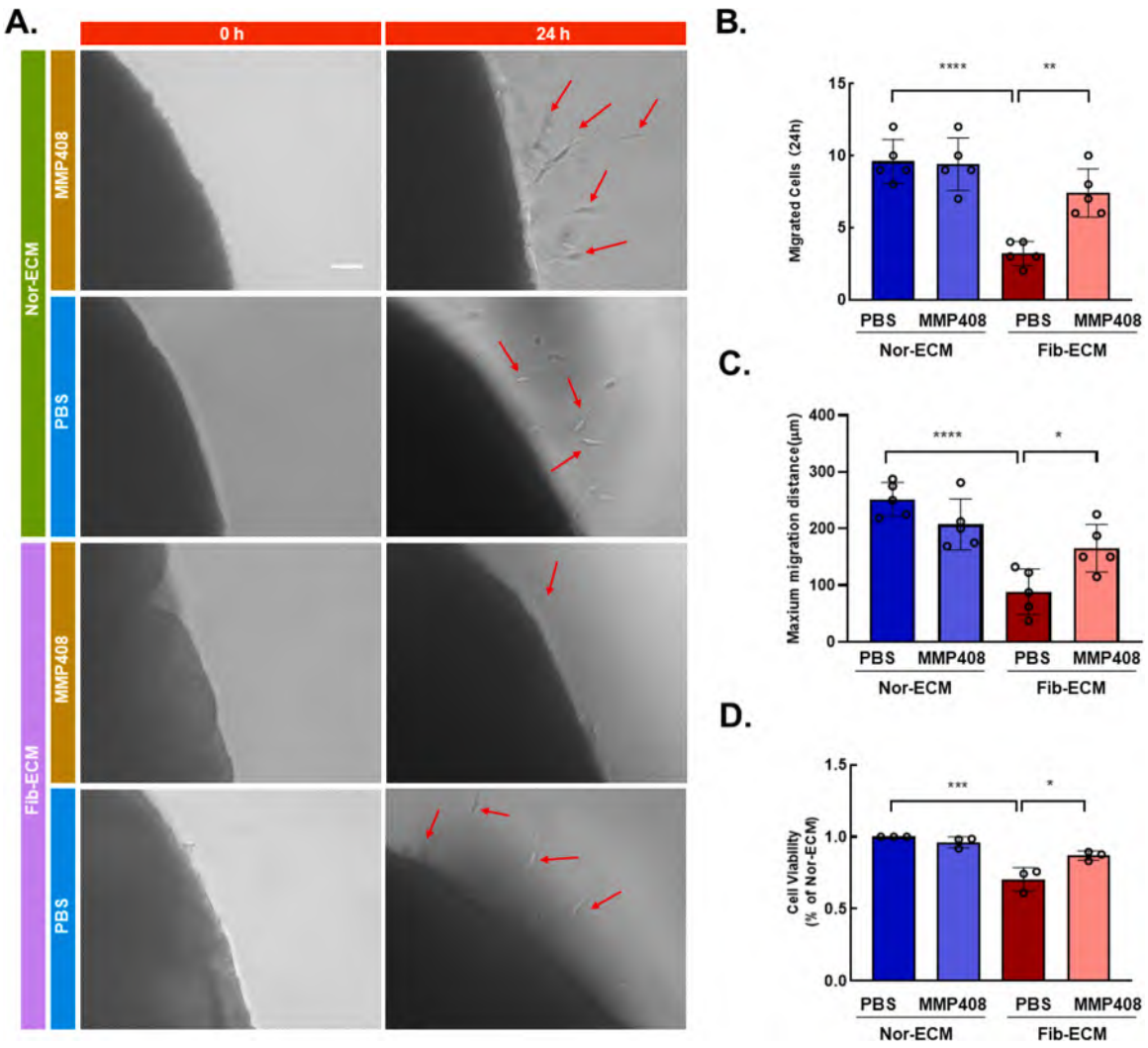

Fig. 8. Endothelial cell dysfunction induced by MMP12 accumulation in ECM. (A) Three-dimensional cell migration assay to detect the effect of MMP12 on fibrosis-like ECM on the migration ability of lung endothelial cells. Scale bar= 100 μm. (B) Statistics of the number of cells migrating out and the maximum distance migrating out in a three-dimensional migration experiment. * ** * $P < 0.0001$ indicates that the number of cell migration as well as the maximum distance were significantly reduced in the Fib-ECM group compared with the Nor-ECM group, * * $P < 0.01$ indicates that in the Fib-ECM group, MMP408 significantly reversed the reduction in cell migration, * $P < 0.05$ indicates that in the Fib-ECM group, MMP408 significantly reversed the maximum distance reduction. (C) * ** $P < 0.001$ indicates a significant decrease in cell viability in the Fib-ECM group compared with the Nor-ECM group, * $P < 0.05$ indicates that in the Fib-ECM group, MMP408 significantly reversed the MMP12-induced decrease in cell viability. Nor-ECM, normal ECM; Fib- ECM, fibrotic ECM. (D) CCK-8 was used to detect the effect of MMP12 on fibrosis-like ECM as indicated by the viability of lung endothelial cells.

[60], as well as the demonstration of large increases in MMP12 in mice with experimentally induced asbestosis [61]. In fibrosis, MMPs exert many biological effects through the degradation of fibronectin, collagens, and other extracellular matrices. In doing so, these proteinases facilitate migration of cells through basement membranes, generate chemotactic gradients, and release growth factors from the matrix environment [62]. It has been suggested that the divergent function of MMP12 in the perivascular and mesenchymal regions during Ang II-induced injury correlates with the presence of M2 macrophages. M2 macrophages can produce profibrotic mediators, including TGFb1 and PDGFBB [63]. Furthermore, fibrosis has been postulated to develop as a consequence of vascular injury, possibly through the production of profibrotic growth factors and cytokines by injured endothelial cells [34]. Additional studies support the notion of too little angiogenesis in pulmonary fibrosis [64-66], which is similar to our findings.

Though we observed that pro-inflammatory macrophage-derived MMP12 was highly expressed in the silica group and was involved in mediating endothelial cell injury, how macrophage polarization and MMP production are related remains unclear. While some studies have found that MMP12 is produced by M2 macrophages, others have shown that M1 macrophages produce MMP12 [67-70]. We found that the expression levels of *Mmp12* were increased in both the early (day 7) and late stages (day 56) of the pathological model. Therefore, we hypothesize that M1 macrophages are primarily responsible for the increased MMP12 in the mouse lungs during the early stages of the disease, whereas M2 macrophages secrete and release some MMP12 during the late stages of the disease, when M1 macrophages undergo apoptotic senescence. We further speculate that macrophage-derived MMP12 may exert a sustained effect in the ECM in the late stage of the pathological model. In general, fibroblasts and epithelial cells profoundly affect the ECM protein composition and mechanical properties of pulmonary fibrosis, but due to ECM-cell crosstalk, fibrosis-like ECM can also influence cell proliferation, migration and differentiation [14-16]. The stiffness of the fibrotic tissue accelerates the development of disease in IPF by modifying gene expression profiles and translational processes in fibroblasts and inducing mechanotransduction pathways [71-74]. Kalafatis et al. [75] discovered that fibroblasts in the ECM can release recruitment factors, causing inflammatory cells such as monocytes and B

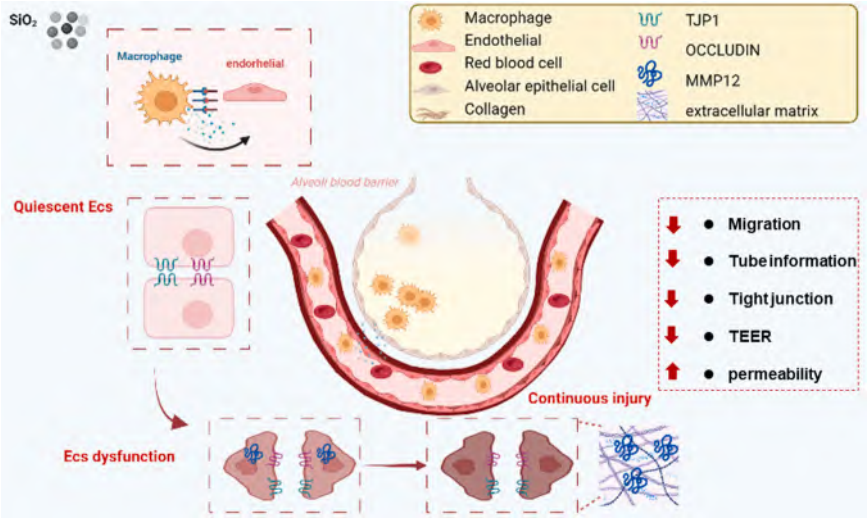

Fig. 9. Effects of macrophage-derived MMP12 on endothelial cell function and mechanisms in the silicosis process.

cells to circulate back to the site of injury. Furthermore, activation of MMP7 can lead to cell infiltration and chronic tissue damage due to the lack of an intact epithelial and endothelial vascular barrier. In our study, MMP12 in fibrosis-like ECM was shown to inhibit the migration and viability of endothelial cells, which was attributed to ECM-cell crosstalk. As a limitation, we were unable to prove that MMP12 accumulation in the ECM can impact the endothelial cell barrier in humans. The cellular microenvironment surrounding fibrotic tissue in mice is different from that in humans, and because our ECM was derived from mice, human-derived ECM will be needed in the future to confirm these results. The present study focused on MMP12 released extracellularly in a secreted form rather than intracellularly, and we therefore used recombinant protein to mimic the effect of secreted protein, which is similar to the approach of another study [76]. In addition, we used an MMP12 inhibitor to block protein function. As a drug target, protein blockade is more advantageous than inhibition of intracellular protein synthesis because it removes the consideration of effects on drug transport across the membrane. However, investigation of MMP12 at the level of protein synthesis also would be worth exploring in future studies to extend the analysis to the regulatory mechanisms of MMP12.

5. Conclusion

This study demonstrates the involvement of MMP12 secreted by macrophages in regulating endothelial cell injury. In this process, pro-inflammatory macrophages secrete MMP12, which can cause endothelial cell injury through cleavage of CDH5, occludin, and TJP1, consequently manifesting as decreased endothelial cell viability, decreased migration, decreased trans endothelial resistance, and increased permeability. We demonstrated that MMP12 deficiency can inhibit these phenomena, and that in the fibrosis phase, macrophage-secreted MMP12 can cause endothelial cell injury through accumulation in the ECM to mediate endothelial cell injury. These results provide insight into mechanisms that may underlie the development of a prevalent and debilitating worldwide disease.

Funding

This work was supported by grants from the National Key Research and Development Program of China (No. 2022YFC2504403) and the National Natural Science Foundation of China (Nos. 82373547, 81972987, 81773796 and 81700068).

CRediT authorship contribution statement

Xinbei Zhou: Validation, investigation, Writing-Original Draft, Data Curation; Cong Zhang: Methodology; Shaoqi Yang, Liliang Yang, Wei Luo: Data Curation; Wei Zhang, Xinxin Zhang: Software; Jie Chao: Design, Data Curation, Writing-Review & Editing.

Declaration of Competing Interest

The authors declare that they have no known competing financial interests or personal relationships that could have appeared to influence the work reported in this paper.

Data availability

Data will be made available on request.

Acknowledgments

We thank LetPub (www.letpub.com) for linguistic assistance and pre-submission expert review.

Appendix A. Supporting information

Supplementary data associated with this article can be found in the online version at doi:10.1016/j.jhazmat.2023.132733.

References

[1] Miao, R., Ding, B., Zhang, Y., Xia, Q., Li, Y., Zhu, B., 2016. Proteomic profiling change during the early development of silicosis disease. J Thorac Dis 8 (3), 329–341. https://doi.org/10.21037/jtd.2016.02.46.
[2] Chen, L., Luo, W., Zhang, W., Chu, H., Wang, J., Dai, X., et al., 2020. circDLPAG4/HECTD1 mediates ischaemia/reperfusion injury in endothelial cells via ER stress. RNA Biol 17 (2), 240–253. https://doi.org/10.1080/15476286.2019.1676114.
[3] Iyer, A.K.V., Ramesh, V., Castro, C.A., Kaushik, V., Kulkarni, Y.M., Wright, C.A., et al., 2015. Nitric oxide mediates bleomycin-induced angiogenesis and pulmonary fibrosis via regulation of VEGF. J Cell Biochem 116 (11), 2484–2493. https://doi.org/10.1002/jcb.25192.
[4] McLoughlin, P., Keane, M.P., 2011. Physiological and pathological angiogenesis in the adult pulmonary circulation. Compr Physiol 1 (3), 473–508. https://doi.org/10.1002/cphy.c100034.
[5] Sun, X., Nkennor, B., Mastikhina, O., Soon, K., Nunes, S.S., 2020. Endothelium-mediated contributions to fibrosis. Semin Cell Dev Biol 101, 78–86. https://doi.org/10.1016/j.semcdb.2019.10.015.
[6] Bagnato, G., Harari, S., 2015. Cellular interactions in the pathogenesis of interstitial lung diseases. Eur Respir Rev 24 (135), 102–114. https://doi.org/10.1183/09059180.00003214.

[7] Byrne, A.J., Maher, T.M., Lloyd, C.M., 2016. Pulmonary macrophages: A new therapeutic pathway in fibrosing lung disease? Trends Mol Med 22 (4), 303–316. https://doi.org/10.1016/j.molmed.2016.02.004.

[8] Aristorena, M., Gallardo-Vara, E., Vicen, M., de Las Casas-Engel, M., Ojeda-Fernandez, L., Nieto, C., et al., 2019. MMP-12, secreted by pro-inflammatory macrophages, targets endoglin in human macrophages and endothelial cells. Int J Mol Sci 20 (12), 3107. https://doi.org/10.3390/ijms20123107.

[9] Kalucka, J., Bierhansl, L., Wielockx, B., Carmeliet, P., Eelen, G., 2017. Interaction of endothelial cells with macrophages—linking molecular and metabolic signaling. Pflüg Arch Eur J Physiol 469 (3–4), 473–483. https://doi.org/10.1007/s00424-017-1946-6.

[10] Cui, N., Hu, M., Khalil, R.A., 2017. Biochemical and biological attributes of matrix metalloproteinases. Prog Mol Biol Transl Sci 147, 1–73. https://doi.org/10.1016/bs.pmbts.2017.02.005.

[11] Craig, V.J., Zhang, L., Hagood, J.S., Owen, C.A., 2015. Matrix metalloproteinases as therapeutic targets for idiopathic pulmonary fibrosis. Am J Respir Cell Mol Biol 53 (5), 585–600. https://doi.org/10.1165/rcmb.2015-0020TR.

[12] Hasaneen, N.A., Cao, J., Pulkoski-Gross, A., Zucker, S., Foda, H.D., 2016. Extracellular Matrix Metalloproteinase Inducer (EMMPRIN) promotes lung fibroblast proliferation, survival and differentiation to myofibroblasts. Respir Res 17, 17. https://doi.org/10.1186/s12931-016-0334-7.

[13] Philp, C.J., Siebeke, I., Clements, D., Miller, S., Habgood, A., John, A.E., et al., 2018. Extracellular matrix cross-linking enhances fibroblast growth and protects against matrix proteolysis in lung fibrosis. Am J Respir Cell Mol Biol 58 (5), 594–603. https://doi.org/10.1165/rcmb.2016-0379oc.

[14] Asano, S., Ito, S., Takahashi, K., Furuya, K., Kondo, M., Sokabe, M., et al., 2017. Matrix stiffness regulates migration of human lung fibroblasts. Physiol Rep 5 (9), e13281. https://doi.org/10.14814/phy2.13281.

[15] Elowsson Rendin, L., Löfdahl, A., Åhrman, E., Müller, C., Notermans, T., Michaliková, B., et al., 2019. Matrisome properties of scaffolds direct fibroblasts in idiopathic pulmonary fibrosis. Int J Mol Sci 20 (16), 4013. https://doi.org/10.3390/ijms20164013.

[16] Haak, A.J., Tan, Q., Tschumperlin, D.J., 2018. Matrix biomechanics and dynamics in pulmonary fibrosis. Matrix Biol 73, 64–76. https://doi.org/10.1016/j.matbio.2017.12.004.

[17] Stuart, T., Butler, A., Hoffman, P., Hafemeister, C., Papalexi, E., Mauck 3rd, W.M., et al., 2019. Comprehensive integration of single-cell data, 1888-1902.e1821 Cell 177 (7). https://doi.org/10.1016/j.cell.2019.05.031.

[18] McGinnis, C.S., Murrow, L.M., Gartner, Z.J., 2019. DoubletFinder: Doublet detection in single-cell RNA sequencing data using artificial nearest neighbors, 329-337.e324 Cell Syst 8 (4). https://doi.org/10.1016/j.cels.2019.03.003.

[19] Korsunsky, I., Millard, N., Fan, J., Slowikowski, K., Zhang, F., Wei, K., et al., 2019. Fast, sensitive and accurate integration of single-cell data with Harmony. Nat Methods 16 (12), 1289–1296. https://doi.org/10.1038/s41592-019-0619-0.

[20] Chrifi, I., Louzao-Martinez, L., Brandt, M.M., van Dijk, C.G.M., Bürgisser, P.E., Zhu, C., et al., 2019. CMTM4 regulates angiogenesis by promoting cell surface recycling of VE-cadherin to endothelial adherens junctions. Angiogenesis 22 (1), 75–93. https://doi.org/10.1007/s10456-018-9638-1.

[21] Felix, K., Tobias, S., Jan, H., Nicolas, S., Michael, M., 2021. Measurements of transepithelial electrical resistance (TEER) are affected by junctional length in immature epithelial monolayers. Histochem Cell Biol 156 (6), 609–616. https://doi.org/10.1007/s00418-021-02026-4.

[22] Kim, D., Eom, S., Park, S.M., Hong, H., Kim, D.S., 2019. A collagen gel-coated, aligned nanofiber membrane for enhanced endothelial barrier function. Sci Rep 9 (1), 14915. https://doi.org/10.1038/s41598-019-51560-8.

[23] Wang, J., Zhang, X., Long, M., Yuan, M., Yin, J., Luo, W., et al., 2023. Macrophage-derived GPNMB trapped by fibrotic extracellular matrix promotes pulmonary fibrosis. Commun Biol 6 (1), 136. https://doi.org/10.1038/s42003-022-04333-5.

[24] Efremova, M., Vento-Tormo, M., Teichmann, S.A., Vento-Tormo, R., 2020. CellPhoneDB: inferring cell–cell communication from combined expression of multi-subunit ligand–receptor complexes. Nat Protoc 15 (4), 1484–1506. https://doi.org/10.1038/s41596-020-0292-x.

[25] Carneiro, P.J., Clevelario, A.L., Padilha, G.A., Silva, J.D., Kitoko, J.Z., Olsen, P.C., et al., 2017. Bosutinib therapy ameliorates lung inflammation and fibrosis in experimental silicosis. Front Physiol 8, 159. https://doi.org/10.3389/fphys.2017.00159.

[26] Piera-Velazquez, S., Mendoza, F.A., Jimenez, S.A., 2016. Endothelial to mesenchymal transition (EndoMT) in the pathogenesis of human fibrotic diseases. J Clin Med 5 (4), 45. https://doi.org/10.3390/jcm5040045.

[27] Liu, X., Qin, X., Qin, H., Jia, C., Yuan, Y., Sun, T., et al., 2021. Characterization of the heterogeneity of endothelial cells in bleomycin-induced lung fibrosis using single-cell RNA sequencing. Angiogenesis 24 (4), 809–821. https://doi.org/10.1007/s10456-021-09795-5.

[28] Aird, W.C., 2007. Phenotypic heterogeneity of the endothelium: I. Structure, function, and mechanisms. Circ Res 100 (2), 158–173. https://doi.org/10.1161/01.res.0000255691.76142.4a.

[29] Magro, C.M., Waldman, W.J., Knight, D.A., Allen, J.N., Nadasdy, T., Frambach, G. E., et al., 2006. Idiopathic pulmonary fibrosis related to endothelial injury and antiendothelial cell antibodies. Hum Immunol 67 (4–5), 284–297. https://doi.org/10.1016/j.humimm.2006.02.026.

[30] Rockey, D.C., Bell, P.D., Hill, J.A., 2015. Fibrosis—A common pathway to organ injury and failure. N Engl J Med 372 (12), 1138–1149. https://doi.org/10.1056/nejmra1300575.

[31] Takabatake, N., Arao, T., Sata, M., Abe, S., Inoue, S., Shibata, Y., et al., 2005. Involvement of pulmonary endothelial cell injury in the pathogenesis of pulmonary fibrosis: clinical assessment by 123I-MIBG lung scintigraphy. Eur J Nucl Med Mol Imaging 32 (2), 221–228. https://doi.org/10.1007/s00259-004-1663-1.

[32] Nardi, J., Nascimento, S., Göethel, G., Gauer, B., Sauer, E., Fão, N., et al., 2018. Inflammatory and oxidative stress parameters as potential early biomarkers for silicosis. Clin Chim Acta 484, 305–313. https://doi.org/10.1016/j.cca.2018.05.045.

[33] Hunt, B.J., Jurd, K.M., 1998. Endothelial cell activation. A central pathophysiological process. BMJ 316 (7141), 1328–1329. https://doi.org/10.1136/bmj.316.7141.1328.

[34] Leach, H.G., Chrobak, I., Han, R., Trojanowska, M., 2013. Endothelial cells recruit macrophages and contribute to a fibrotic milieu in bleomycin lung injury. Am J Respir Cell Mol Biol 49 (6), 1093–1101. https://doi.org/10.1165/rcmb.2013-0152OC.

[35] Pakshir, P., Hinz, B., 2018. The big five in fibrosis: Macrophages, myofibroblasts, matrix, mechanics, and miscommunication. Matrix Biol 68–69, 81–93. https://doi.org/10.1016/j.matbio.2018.01.019.

[36] Ballermann, B.J., Obeidat, M., 2014. Tipping the balance from angiogenesis to fibrosis in CKD (2011). Kidney Int Suppl 4 (1), 45–52. https://doi.org/10.1038/kisup.2014.9.

[37] Basile, D.P., 2008. Challenges of targeting vascular stability in acute kidney injury. Kidney Int 74 (3), 257–258. https://doi.org/10.1038/ki.2008.243.

[38] Casazza, A., Laoui, D., Wenes, M., Rizzolio, S., Bassani, N., Mambretti, M., et al., 2013. Impeding macrophage entry into hypoxic tumor areas by Sema3A/Nrp1 signaling blockade inhibits angiogenesis and restores antitumor immunity. Cancer Cell 24 (6), 695–709. https://doi.org/10.1016/j.ccr.2013.11.007.

[39] Ehling, J., Bartneck, M., Wei, X., Gremse, F., Fech, V., Möckel, D., et al., 2014. CCL2-dependent infiltrating macrophages promote angiogenesis in progressive liver fibrosis. Gut 63 (12), 1960–1971. https://doi.org/10.1136/gutjnl-2013-306294.

[40] Liu, H., Fang, S., Wang, W., Cheng, Y., Zhang, Y., Liao, H., et al., 2016. Macrophage-derived MCPIP1 mediates silica-induced pulmonary fibrosis via autophagy. Part Fibre Toxicol 13 (1), 55. https://doi.org/10.1186/s12989-016-0167-z.

[41] Liu, H., Cheng, Y., Yang, J., Wang, W., Fang, S., Zhang, W., et al., 2017. BBC3 in macrophages promoted pulmonary fibrosis development through inducing autophagy during silicosis. Cell Death Dis 8, e2657. https://doi.org/10.1038/cddis.2017.78.

[42] Zhou, Z., Jiang, R., Yang, X., Guo, H., Fang, S., Zhang, Y., et al., 2018. circRNA Mediates Silica-Induced Macrophage Activation Via HECTD1/ZC3H12A-Dependent Ubiquitination. Theranostics 8, 575–592. https://doi.org/10.7150/thno.21648.

[43] Yang, X., Wang, J., Zhou, Z., Jiang, R., Huang, J., Chen, L., et al., 2018. Silica-induced initiation of circular ZC3H4 RNA/ZC3H4 pathway promotes the pulmonary macrophage activation. FASEB J 32 (6), 3264–3277. https://doi.org/10.1096/fj.201701118R.

[44] Wang X., Zhang Y., Zhang W., Liu H., Zhou Z., Dai X., et al. MCPIP1 Regulates Alveolar Macrophage Apoptosis and Pulmonary Fibroblast Activation After in vitro Exposure to Silica. *Toxicol Sci* 151(1):126–138. doi:10.1093/toxsci/kfw029.

[45] Zhang, W., Zhang, M., Wang, Z., Cheng, Y., Liu, H., Zhou, Z., et al., 2016. Neogambogic acid prevents silica-induced fibrosis via inhibition of high-mobility group bo***x 1 and MCP-1-induced protein 1***. Toxicol Appl Pharmacol 309, 129–140. https://doi.org/10.1016/j.taap.2016.09.003.

[46] Farley, K.S., Wang, L., Mehta, S., 2009. Septic pulmonary microvascular endothelial cell injury: role of alveolar macrophage NADPH oxidase. Am J Physiol Lung Cell Mol Physiol 296 (3), L480–L488. https://doi.org/10.1152/ajplung.90201.2008.

[47] Roy, A., Saqib, U., Baig, M.S., 2021. NOS1–mediated macrophage and endothelial cell interaction in the progression of atherosclerosis. Cell Biol Int 45 (6), 1191–1201. https://doi.org/10.1002/cbin.11558.

[48] Tusavitz, S., Keoonela, S., Kalkstein, M., McCormick, S., Gasser, B., Arrigale, M., et al., 2020. Macrophage-derived Wnt signaling increases endothelial permeability during skeletal muscle injury. Inflamm Res 69 (12), 1235–1244. https://doi.org/10.1007/s00011-020-01397-z.

[49] McCourtie, A.S., Merry, H.E., Farivar, A.S., Goss, C.H., Mulligan, M.S., 2008. Alveolar macrophage secretory products augment the response of rat pulmonary artery endothelial cells to hypoxia and reoxygenation. Ann Thorac Surg 85 (3), 1056–1060. https://doi.org/10.1016/j.athoracsur.2007.10.058.

[50] Chen, Q., Jin, M., Yang, F., Zhu, J., Xiao, Q., Zhang, L., 2013. Matrix metalloproteinases: inflammatory regulators of cell behaviors in vascular formation and remodeling. Mediat Inflamm 2013, 928315. https://doi.org/10.1155/2013/928315.

[51] Inoue, T., Sata, M., Hikichi, Y., Sohma, R., Fukuda, D., Uchida, T., et al., 2007. Mobilization of CD34-positive bone marrow–derived cells after coronary stent implantation. Circulation 115 (5), 553–561. https://doi.org/10.1161/circulationaha.106.621714.

[52] Inoue, T., Taguchi, I., Abe, S., Toyoda, S., Nakajima, K., Sakuma, M., et al., 2011. Activation of matrix metalloproteinase-9 is associated with mobilization of bone marrow-derived cells after coronary stent implantation. Int J Cardiol 152 (3), 332–336. https://doi.org/10.1016/j.ijcard.2010.07.028.

[53] Guan, C., Xiao, Y., Li, K., Wang, T., Liang, Y., Liao, G., 2019. MMP-12 regulates proliferation of mouse macrophages via the ERK/P38 MAPK pathways during inflammation. Exp Cell Res 378 (2), 182–190. https://doi.org/10.1016/j.yexcr.2019.03.018.

[54] Wu, L., Fan, J., Matsumoto, S.-I., Watanabe, T., 2000. Induction and regulation of matrix metalloproteinase-12 by cytokines and CD40 signaling in monocyte/

macrophages. Biochem Biophys Res Commun 269 (3), 808–815. https://doi.org/10.1006/bbrc.2000.2368.
[55] Chaudhuri, R., McSharry, C., Brady, J., Donnelly, I., Grierson, C., McGuinness, S., et al., 2012. Sputum matrix metalloproteinase-12 in patients with chronic obstructive pulmonary disease and asthma: Relationship to disease severity, 655–663.e658 J Allergy Clin Immunol 129 (3). https://doi.org/10.1016/j.jaci.2011.12.996.
[56] Manetti, M., Guiducci, S., Romano, E., Bellando-Randone, S., Conforti, M.L., Ibba-Manneschi, L., et al., 2012. Increased serum levels and tissue expression of matrix metalloproteinase-12 in patients with systemic sclerosis: correlation with severity of skin and pulmonary fibrosis and vascular damage. Ann Rheum Dis 71 (6), 1064–1072. https://doi.org/10.1136/annrheumdis-2011-200837.
[57] Houghton, A.M., Grisolano, J.L., Baumann, M.L., Kobayashi, D.K., Hautamaki, R. D., Nehring, L.C., et al., 2006. Macrophage elastase (matrix metalloproteinase-12) suppresses growth of lung metastases. Cancer Res; 66 (12), 6149–6155. https://doi.org/10.1158/0008-5472.CAN-04-0297.
[58] Acuff, H.B., Sinnamon, M., Fingleton, B., Boone, B., Levy, S.E., Chen, X., et al., 2006. Analysis of host- and tumor-derived proteinases using a custom dual species microarray reveals a protective role for stromal matrix metalloproteinase-12 in non-small cell lung cancer. Cancer Res 66 (16), 7968–7975. https://doi.org/10.1158/0008-5472.CAN-05-4279.
[59] Cornelius, L.A., Nehring, L.C., Harding, E., Bolanowski, M., Welgus, H.G., Kobayashi, D.K., et al., 1998. Matrix metalloproteinases generate angiostatin: effects on neovascularization. J Immunol 161 (12), 6845–6852.
[60] Todd, J.L., Vinisko, R., Liu, Y., Neely, M.L., Overton, R., Flaherty, K.R., 2020. Circulating matrix metalloproteinases and tissue metalloproteinase inhibitors in patients with idiopathic pulmonary fibrosis in the multicenter IPF-PRO Registry cohort. BMC Pulm Med 20 (1), 64. https://doi.org/10.1186/s12890-020-1103-4.
[61] Tan, R.J., Fattman, C.L., Niehouse, L.M., Tobolewski, J.M., Hanford, L.E., Li, Q., et al., 2006. Matrix metalloproteinases promote inflammation and fibrosis in asbestos-induced lung injury in mice. Am J Respir Cell Mol Biol 35 (3), 289–297. https://doi.org/10.1165/rcmb.2005-0471OC.
[62] Roman, J., 2017. On the "TRAIL" of a Killer: MMP12 in Lung Cancer. Am J Respir Crit Care Med 196 (3), 262–264. https://doi.org/10.1164/rccm.201704-0668ED.
[63] Stawski, L., Haines, P., Fine, A., Rudnicka, L., Trojanowska, M., 2014. MMP-12 deficiency attenuates angiotensin II-induced vascular injury, M2 macrophage accumulation, and skin and heart fibrosis. PLoS One 9 (10), e109763. https://doi.org/10.1371/journal.pone.0109763 eCollection 2014.
[64] Ebina, M., Shimizukawa, M., Shibata, N., Kimura, Y., Suzuki, T., Endo, M., 2004. Heterogeneous increase in CD34-positive alveolar capillaries in idiopathic pulmonary fibrosis. Am J Respir Crit Care Med 169 (11), 1203–1208. https://doi.org/10.1164/rccm.200308-1111OC.
[65] Cosgrove, G.P., Brown, K.K., Schiemann, W.P., Serls, A.E., Parr, J.E., Geraci, M.W., et al., 2004. Pigment epithelium-derived factor in idiopathic pulmonary fibrosis: a role in aberrant angiogenesis. Am J Respir Crit Care Med 170 (3), 242–251. https://doi.org/10.1164/rccm.200308-1151OC.
[66] Sumi, M., Satoh, H., Kagohashi, K., Ishikawa, H., Sekizawa, K., 2005. Increased serum levels of endostatin in patients with idiopathic pulmonary fibrosis. J Clin Lab Anal 19 (4), 146–149. https://doi.org/10.1002/jcla.20069.
[67] Butcher, M.J., Galkina, E.V., 2012. Phenotypic and functional heterogeneity of macrophages and dendritic cell subsets in the healthy and atherosclerosis-prone aorta. Front Physiol 3, 44. https://doi.org/10.3389/fphys.2012.00044.
[68] Hiemstra, P.S., 2013. Altered macrophage function in chronic obstructive pulmonary disease. Ann Am Thorac Soc 10 (Supplement), S180–S185. https://doi.org/10.1513/annalsats.201305-123aw.
[69] Stahl, E.C., Haschak, M.J., Popovic, B., Brown, B.N., 2018. Macrophages in the aging liver and age-related liver disease. Front Immunol 9, 2795. https://doi.org/10.3389/fimmu.2018.02795.
[70] Vlahos, R., Bozinovski, S., 2014. Role of alveolar macrophages in chronic obstructive pulmonary disease. Front Immunol 5, 435. https://doi.org/10.3389/fimmu.2014.00435.
[71] Berhan, A., Harris, T., Jaffar, J., Jativa, F., Langenbach, S., Lönnstedt, I., et al., 2020. Cellular microenvironment stiffness regulates eicosanoid production and signaling pathways. Am J Respir Cell Mol Biol 63 (6), 819–830. https://doi.org/10.1165/rcmb.2020-0227oc.
[72] Herrera, J., Forster, C., Pengo, T., Montero, A., Swift, J., Schwartz, M.A., et al., 2019. Registration of the extracellular matrix components constituting the fibroblastic focus in idiopathic pulmonary fibrosis. JCI Insight 4 (1), e125185. https://doi.org/10.1172/jci.insight.125185.
[73] Liu, F., Lagares, D., Choi, K.M., Stopfer, L., Marinković, A., Vrbanac, V., et al., 2015. Mechanosignaling through YAP and TAZ drives fibroblast activation and fibrosis. Am J Physiol Lung Cell Mol Physiol 308 (4), L344–L357. https://doi.org/10.1152/ajplung.00300.2014.
[74] Parker, M.W., Rossi, D., Peterson, M., Smith, K., Sikström, K., White, E.S., et al., 2014. Fibrotic extracellular matrix activates a profibrotic positive feedback loop. J Clin Invest 124 (4), 1622–1635. https://doi.org/10.1172/JCI71386.
[75] Kalafatis, D., Löfdahl, A., Näsman, P., Dellgren, G., Wheelock, Å.M., Elowsson Rendin, L., et al., 2021. Distal lung microenvironment triggers release of mediators recognized as potential systemic biomarkers for idiopathic pulmonary fibrosis. Int J Mol Sci 22 (24), 13421. https://doi.org/10.3390/ijms222413421.
[76] Nénan, S., Lagente, V., Planquois, J.M., Hitier, S., Berna, P., et al., 2007. Metalloelastase (MMP-12) induced inflammatory response in mice airways: effects of dexamethasone, rolipram and marimastat. Eur J Pharmacol 559 (1), 75–81. https://doi.org/10.1016/j.ejphar.2006.11.070.